Robust circadian clocks from coupled protein-modification and transcription–translation cycles

David Zwicker[a,1], David K. Lubensky[b,2], and Pieter Rein ten Wolde[a,2]

[a]FOM (Stichting voor Fundamenteel Onderzoek der Materie) Institute for Atomic and Molecular Physics (AMOLF), Science Park 104, 1098 XG Amsterdam, The Netherlands; and [b]Department of Physics, University of Michigan, Ann Arbor, MI 48109-1040

Edited by David R. Nelson, Harvard University, Cambridge, MA, and approved November 2, 2010 (received for review May 31, 2010)

The cyanobacterium *Synechococcus elongatus* uses both a protein phosphorylation cycle and a transcription–translation cycle to generate circadian rhythms that are highly robust against biochemical noise. We use stochastic simulations to analyze how these cycles interact to generate stable rhythms in growing, dividing cells. We find that a protein phosphorylation cycle by itself is robust when protein turnover is low. For high decay or dilution rates (and compensating synthesis rates), however, the phosphorylation-based oscillator loses its integrity. Circadian rhythms thus cannot be generated with a phosphorylation cycle alone when the growth rate, and consequently the rate of protein dilution, is high enough; in practice, a purely posttranslational clock ceases to function well when the cell doubling time drops below the 24-h clock period. At higher growth rates, a transcription–translation cycle becomes essential for generating robust circadian rhythms. Interestingly, although a transcription–translation cycle is necessary to sustain a phosphorylation cycle at high growth rates, a phosphorylation cycle can dramatically enhance the robustness of a transcription–translation cycle at lower protein decay or dilution rates. In fact, the full oscillator built from these two tightly intertwined cycles far outperforms not just each of its two components individually, but also a hypothetical system in which the two parts are coupled as in textbook models of coupled phase oscillators. Our analysis thus predicts that both cycles are required to generate robust circadian rhythms over the full range of growth conditions.

Kai | oscillations

Many organisms use circadian clocks to anticipate changes between day and night (1). It had long been believed that these clocks are driven primarily by transcription–translation cycles built on negative feedback. However, although some circadian clocks can maintain robust rhythms for years in the absence of any daily cue (1), recent experiments have vividly demonstrated that gene expression is often highly stochastic (2). This raises the question of how these clocks can be so robust against biochemical noise. In multicellular organisms, the robustness might be explained by intercellular interactions (3, 4), but it is now known that even unicellular organisms can have very stable circadian rhythms. The clock of the cyanobacterium *Synechococcus elongatus*, for example, has a correlation time of several months (5), even though the clocks of the different cells in a population hardly interact with one another (5, 6). How circadian clocks can be so stable even at the single cell level is not understood.

Interestingly, it has recently been discovered that the *S. elongatus* clock combines a transcription–translation cycle (TTC) with a protein phosphorylation cycle (PPC). The central components of the clock are the three genes *kaiA*, *kaiB*, and *kaiC* (7). Under continuous light conditions, the levels of mRNA from the *kaiBC* operon and of the protein KaiC oscillate in a circadian fashion (8); moreover, overexpression of KaiC abolishes *kaiBC* expression (9, 10). These observations led to the proposal that the Kai system is a transcription–translation oscillator, with KaiC negatively regulating its own transcription. In 2005, however, Kondo and coworkers showed that KaiC, which is a hexamer with two phosphorylation sites per monomer (11), is phosphorylated in a cyclical manner with a period of 24 h, even when *kaiBC* transcription is inhibited (12). Still more remarkably, the rhythmic phosphorylation of KaiC could be reconstituted in the test tube in the presence of only KaiA, KaiB, and ATP (13). This raised the possibility that the principal pacemaker of the clock is not a TTC, but a PPC (13). Yet, in 2008, the same group showed that circadian oscillations of gene expression persist even when KaiC is always held in a highly phosphorylated state (14). They thus concluded that the clock is driven by both a TTC and a PPC and suggested that the interactions between the two oscillators may enhance the robustness of the clock (14).

Here, we use mathematical modeling to study how a protein-modification oscillator and a transcription–translation oscillator interact in growing, dividing cells. To this end, we study four models, schematically shown in Fig. 1: (*i*) *PPC-in vitro* model (Fig. 1*B*); (*ii*) *PPC-in vivo* model (Fig. 1*C*); (*iii*) *PPC-TTC* model (Fig. 1*A*); (*iv*) *TTC-only* model (Fig. 1*D*). We first study the *PPC-in vitro* model, which describes the PPC that has been reconstituted in the test tube (13) (Fig. 1*B*). In this system, the total number of each Kai protein is *constant*—they are neither produced nor destroyed—and only the PPC is operative. We show that in this case the PPC is highly robust against noise arising from the intrinsic stochasticity of chemical reactions. Even for reaction volumes smaller than the typical volume of a cyanobacterium, the correlation time is longer than that observed experimentally (5). Living cells, however, constantly grow and divide, and proteins must thus be synthesized to balance dilution. In fact, dilution can be thought of as introducing an effective protein degradation rate set by the cell doubling time. We therefore next study the *PPC-in vivo* model (Fig. 1*C*), which describes a PPC in which the Kai proteins are produced and degraded with rates that are constant in time. The simulations reveal that protein synthesis and decay dramatically reduce the viability of the PPC; we predict that for a cell doubling time of 24 h and a bacterial volume of 1 μm^3, the PPC dephases in roughly 10 days, much faster than real *S. elongatus* (5). This is because the constant synthesis of proteins, which we assume are all initially created in the same phosphorylation state, necessarily injects KaiC with the "wrong" phosphorylation level at certain phases of the cycle (1, 15, 16); if these appear fast enough, they can destroy the oscillation. One role of the TTC is thus to introduce proteins only when the phosphorylation state of the freshly made KaiC matches that of the PPC. Our simulations of the *PPC-TTC* model (Fig. 1*A*), which combines a PPC and a TTC, reveal that a TTC can indeed greatly

Author contributions: D.Z., D.K.L., and P.R.t.W. designed research, performed research, analyzed data, and wrote the paper.

The authors declare no conflict of interest.

This article is a PNAS Direct Submission.

[1]Present address: Max Planck Institute for the Physics of Complex Systems, Nöthnitzer Strasse 38, 01187 Dresden, Germany.

[2]To whom correspondence may be addressed. E-mail: dkluben@umich.edu or tenwolde@amolf.nl.

This article contains supporting information online at www.pnas.org/lookup/suppl/doi:10.1073/pnas.1007613107/-/DCSupplemental.

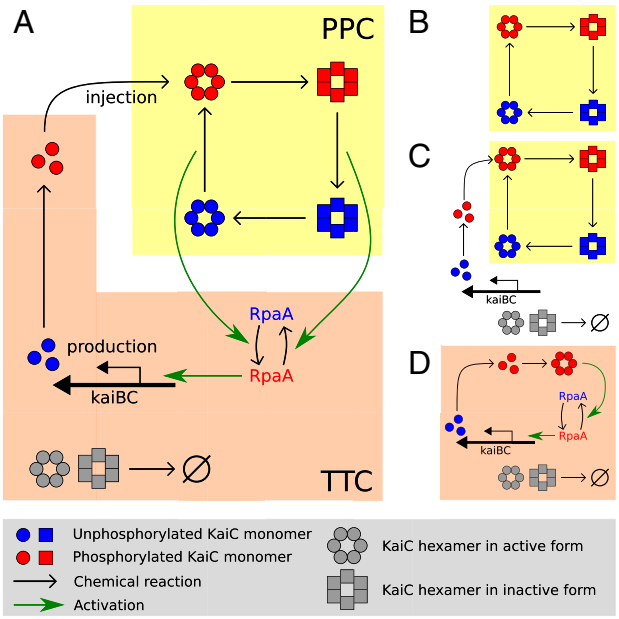

Fig. 1. Overview of the models studied in this manuscript. (*A*) *PPC-TTC* model: A TTC of *kaiBC* expression (orange background) interacts with a KaiC PPC (yellow background) (40). KaiC is a hexamer that, in our model, switches between an active conformational state (circles) in which its phosphorylation level tends to rise and an inactive state (squares) in which it tends to fall. Active KaiC activates RpaA, whereas inactive KaiC inactivates RpaA; active RpaA (red) activates *kaiBC* expression, leading (after a delay) to the injection of fully phosphorylated KaiC into the PPC. (*B*) *PPC-in vitro* model: Only the PPC is present, and the concentration of each Kai protein is constant. (*C*) *PPC-in vivo* model: Only the PPC is present, but all Kai proteins are now continually synthesized and degraded, with rates that are constant in time. (*D*) *TTC-only* model: Only the TTC is present, and KaiC is always in a highly phosphorylated state. *RpaA* and *kaiA* are expressed constitutively; roles of KaiA and KaiB are discussed in the text.

enhance the robustness of the PPC, yielding correlation times consistent with those measured experimentally (5). Finally, we consider whether the PPC is needed at all, or whether one could build an equally good circadian clock using only a TTC; to this end, we study the *TTC-only* model (Fig. 1*D*). We find that it is possible to construct a TTC with a period of 24 h and the observed correlation time of a few months (5). However, this comes at the expense of very high protein synthesis and decay rates, which impose an extra energetic burden on the cell. Our results thus suggest that a PPC allows for a more robust oscillator at a lower cost. Although our models are simplified, we argue in *Principal Pacemaker* and *Discussion* that our qualitative results are unavoidable consequences of the interaction between a circadian clock and cell growth and so should hold far more generally.

Results

A. *PPC-in Vitro*: A Protein Phosphorylation Cycle with Constant Protein Concentrations Is Highly Robust. The PPC has been characterized in detail (Fig. 1*B*). KaiC forms a hexamer (11) with two phosphorylation sites per protein monomer, which are phosphorylated and dephosphorylated in a definite sequence as a result of KaiC's autokinase and autophosphatase activity (17, 18). KaiA stimulates KaiC phosphorylation (19, 20), whereas KaiB negates the effect of KaiA (19–22). Thanks to the wealth of available experimental data, the PPC has proven a fruitful system for mathematical modeling (18, 23–31) (for a review, see ref. 32).

In this manuscript, we adopt the mathematical model developed by us (26). In this model, each KaiC hexamer has an intrinsic ability to cyclically phosphorylate and dephosphorylate itself, while the phosphorylation cycles of the individual hexamers are synchronized via a mechanism that we called "differential affinity" (18, 23, 26, 27): KaiA stimulates KaiC phosphorylation, but the limited supply of KaiA dimers binds preferentially to those KaiC molecules that are falling behind in the cycle, allowing them to catch up. Specifically, in our model each KaiC hexamer can switch between an active conformational state C_i, where the number i of phosphorylated monomers tends to increase, and an inactive state $\tilde{C}_i$, where i tends to decrease (Fig. 1*B*); KaiA stimulates phosphorylation of active KaiC, but is sequestered by complexes containing KaiB and inactive KaiC. KaiC in the inactive state can thus delay the progress of fully dephosphorylated hexamers that have already switched back to the active state and are ready to be phosphorylated again. With A and B denoting, respectively, a KaiA dimer and a KaiB dimer, the model becomes

$$\mathrm{C}_i \underset{b_i}{\overset{f_i}{\rightleftarrows}} \tilde{\mathrm{C}}_i, \qquad \mathrm{C}_i + \mathrm{A} \underset{k_i^{\mathrm{Ab}}}{\overset{k_i^{\mathrm{Af}}}{\rightleftarrows}} \mathrm{AC}_i \overset{k_{\mathrm{pf}}}{\rightarrow} \mathrm{C}_{i+1} + \mathrm{A}, \qquad [1]$$

$$\tilde{\mathrm{C}}_i + \mathrm{B} \underset{\tilde{k}_i^{\mathrm{Bb}}}{\overset{2\tilde{k}_i^{\mathrm{Bf}}}{\rightleftarrows}} \mathrm{B}\tilde{\mathrm{C}}_i, \qquad \mathrm{B}\tilde{\mathrm{C}}_i + \mathrm{B} \underset{2\tilde{k}_i^{\mathrm{Bb}}}{\overset{\tilde{k}_i^{\mathrm{Bf}}}{\rightleftarrows}} \mathrm{B}_2\tilde{\mathrm{C}}_i, \qquad [2]$$

$$\mathrm{B}_x\tilde{\mathrm{C}}_i + \mathrm{A} \underset{\tilde{k}_i^{\mathrm{Ab}}}{\overset{x\tilde{k}_i^{\mathrm{Af}}}{\rightleftarrows}} \mathrm{AB}_x\tilde{\mathrm{C}}_i, \qquad \mathrm{AB}_2\tilde{\mathrm{C}}_i + \mathrm{A} \underset{2\tilde{k}_i^{\mathrm{Ab}}}{\overset{\tilde{k}_i^{\mathrm{Af}}}{\rightleftarrows}} \mathrm{A}_2\mathrm{B}_2\tilde{\mathrm{C}}_i, \qquad [3]$$

$$\mathrm{C}_i \underset{k_{\mathrm{dps}}}{\overset{k_{\mathrm{ps}}}{\rightleftarrows}} \mathrm{C}_{i+1}, \qquad \tilde{\mathrm{C}}_i \underset{\tilde{k}_{\mathrm{dps}}}{\overset{\tilde{k}_{\mathrm{ps}}}{\rightleftarrows}} \tilde{\mathrm{C}}_{i+1}, \qquad [4]$$

$$\mathrm{B}_x\tilde{\mathrm{C}}_i \underset{\tilde{k}_{\mathrm{dps}}}{\overset{\tilde{k}_{\mathrm{ps}}}{\rightleftarrows}} \mathrm{B}_x\tilde{\mathrm{C}}_{i+1}, \qquad \mathrm{A}_y\mathrm{B}_x\tilde{\mathrm{C}}_i \underset{\tilde{k}_{\mathrm{dps}}}{\overset{\tilde{k}_{\mathrm{ps}}}{\rightleftarrows}} \mathrm{A}_y\mathrm{B}_x\tilde{\mathrm{C}}_{i+1}. \qquad [5]$$

This model reproduces the phosphorylation behavior of KaiC in vitro not only when all Kai proteins are present, but also when KaiA and/or KaiB are absent (26). It moreover correctly predicted the experimentally observed disappearance of oscillations when the KaiA concentration is raised (18, 33), a success that strongly supports the idea that KaiA sequestration is the primary driver of synchronization. Our model does not feature monomer exchange between KaiC hexamers, an alternative means of synchronization (24) that has been observed in experiments (28, 34); we and others find that monomer exchange is not critical for stable oscillations (18, 26, 27). In *SI Text*, we show that similar results are obtained with a model that focuses on the phosphorylation cycle of individual KaiC monomers (17, 18) rather than of KaiC hexamers.

We quantify our model's robustness to chemical noise by performing Monte Carlo simulations of the chemical master equation (35) describing the mass-action kinetics associated with reactions **1–5** in a well-mixed container. In our simulations, we vary the reaction volume V but adjust the protein copy numbers so that the concentrations of the Kai proteins remain constant, at levels comparable to those used in vitro (33, 34). Fig. 2 shows as a function of volume the correlation number of cycles $n_{1/2}$, defined as the number of cycles after which the standard deviation in the phase of the oscillation is half a day (31). One issue that arises in comparing our results to the measured in vivo clock robustness is that the Kai proteins appear to be present in living cells in a ratio at which the in vitro system would not oscillate (21, 33, 34). It has been suggested that this discrepancy may indicate that the clock reactions are confined to a subdomain of the cell from which some KaiB and KaiC molecules are excluded (21), allowing the reactions to proceed at roughly the in vitro ratio (see *SI Text*). If we take the volume of this domain to be $V \sim 1\ \mu\mathrm{m}^3$, comparable to the size of the entire cell, then Fig. 2 shows that $n_{1/2} \approx 200$, consistent with the measured 166 ± 100 (5). Even for $V \sim 0.5\ \mu\mathrm{m}^3$, we find that $n_{1/2} \approx 102$, still within the experimental bounds (in contrast to predictions of some alternative

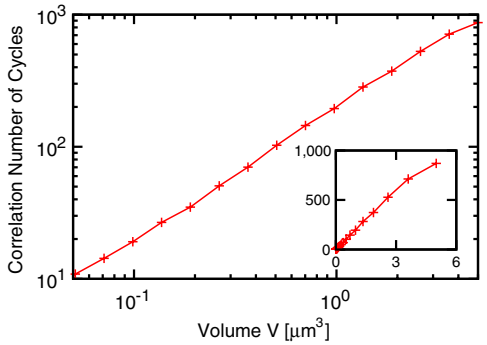

Fig. 2. *PPC-in vitro* model (Fig. 1*B*). Correlation number of cycles, $n_{1/2}$, as a function of the reaction volume V. For $V \approx 1$ μm^3, comparable to the size of a cyanobacterium, $n_{1/2} \approx 200$, in agreement with experiment (5). (*Inset*) The same data on a linear scale. The protein concentrations are those used in the in vitro experiments (33, 34): $[A]_T = 0.58$ μM; $[B]_T = 1.75$ μM; $[C]_T = 0.58$ μM. For other parameters, see Table S1. For a time trace of the phosphorylation level $p(t)$, see Fig. S1.

models (18, 31); see *SI Text*). Our model thus predicts that the PPC is resistant to noise arising from the stochastic nature of chemical reactions.

B. *PPC-in Vivo*: A Phosphorylation Cycle with Constant Protein Synthesis and Degradation Rates Is not Stable. Fig. 2 shows that the PPC is highly robust when the total concentrations of the Kai proteins are strictly constant. But, in vivo, proteins are continually being synthesized and degraded. To study how this affects the PPC, we consider the *PPC-in vivo* model (Fig. 1*C*). In this model, the Kai proteins are produced and degraded in a stochastic (memoryless) fashion with rates that are constant in time, with the effects of active degradation (36) and of passive dilution lumped into a single first-order decay rate μ (see *SI Text*).

Fig. 3 shows the performance of the PPC as a function of degradation rate and cell volume; here, and in the models below, the synthesis rates are adjusted so that the mean concentrations are constant and equal to those used in the previous section. The PPC's robustness clearly decreases dramatically with increasing protein synthesis and decay rate. For a volume comparable to that of a cyanobacterium and a degradation rate of 0.03 h^{-1}, the correlation time is less than 20 days, much lower than that observed in vivo (5). This degradation rate is precisely the effective rate arising from protein dilution with a cell doubling time of 24 h. It is known, however, that KaiC is also degraded actively at a rate as high as 0.1 h^{-1} (36), leading to still worse stability.

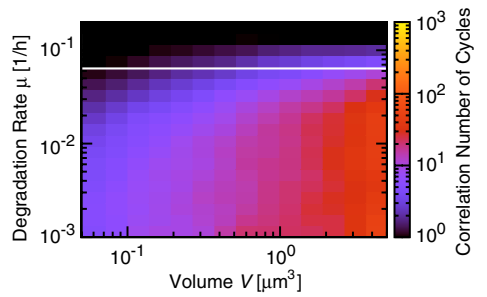

Fig. 3. *PPC-in vivo* model (Fig. 1*C*). Correlation number of cycles, $n_{1/2}$, as a function of reaction volume V and degradation rate μ. $n_{1/2}$ decreases as μ increases. Thus, a system in which the Kai proteins are produced and degraded with constant rates cannot sustain a stable phosphorylation cycle when the growth rate is high. The bifurcation line $\mu = 0.0621$ h^{-1}, where the system undergoes a supercritical Hopf bifurcation in the deterministic limit, is shown in white. KaiA, KaiB, and KaiC are produced with rates such that the average total concentrations equal those used in the in vitro experiments (see Fig. 2). For a time trace of $p(t)$, see Fig. S1.

The disappearance of the oscillations for higher protein synthesis and decay rates can be understood by noting that fresh KaiC hexamers are made in a fixed phosphorylation state, which then has to catch up with that of the proteins already in the cycle (1, 15). When the degradation rate is high, the new proteins are likely to be degraded before the PPC can synchronize their phosphorylation levels; indeed, in the limit that the protein synthesis and decay rates go to infinity, the phosphorylation level $p(t)$ (defined as the fraction of phosphorylated monomers) becomes constant in time and equal to the phosphorylation level of freshly made KaiC proteins. This is not a purely stochastic effect; the white bifurcation line of Fig. 3 shows that even in a deterministic model the oscillations disappear when the synthesis and decay rates become too big (see *SI Text*).

C. *PPC-TTC*: A Protein Phosphorylation Cycle with a Transcription–Translation Cycle Is very Stable. To sustain a phosphorylation cycle, KaiC has to be made in an oscillatory fashion: Newly synthesized KaiC proteins should be injected into the phosphorylation cycle only when their phosphorylation state matches that of the PPC as a whole (1). This is the principal role of the transcription–translation cycle. Here, we present a mathematical model, the *PPC-TTC* model, for how such a cycle might interact with the PPC (Fig. 1*A*).

Although the TTC is much less well understood than the PPC, recently much progress has been made (37–39). In particular, several proteins important for transcriptional regulation of the *kaiBC* operon have now been identified. Our model is inspired by that of Taniguchi et al. (40) and contains the following key ingredients:

1. RpaA activates kaiBC expression. Deletion of *rpaA*, which encodes a putative response regulator, reduces *kaiBC* expression (40–42). Because neither promoters nor transcription or chromosome-compaction factors have been identified that interact with RpaA (42), we make the phenomenological assumption that RpaA directly activates *kaiBC* expression (40).

2. RpaA is activated by KaiC when KaiC is in the active state. RpaA is activated via phosphorylation by the histidine kinase SasA, whose activity is in turn stimulated by KaiC (38, 42); inactivation of SasA reduces *kaiBC* expression (40–42). Moreover, RpaA phosphorylation occurs 4–8 h before the peak of KaiC phosphorylation (42). This suggests that partially phosphorylated KaiC that is on the PPC's active branch activates RpaA through SasA (40). Because SasA phosphorylation, occurring on time scales of minutes (38), is much faster than KaiC phosphorylation, occurring on time scales of hours, we assume that the SasA dynamics can be integrated out.

3. RpaA is inactivated by KaiC when KaiC is in the inactive state. Inactivation of LabA (41) or CikA (40) increases *kaiBC* expression, with inactivation of both having a still stronger effect (40). SasA inactivation can compensate for both LabA (41) and CikA inactivation (40), but RpaA inactivation cannot compensate for LabA inactivation (41). Taken together, these results suggest that SasA, LabA, and CikA control *kaiBC* expression through different pathways, with at least the SasA and LabA pathways converging on RpaA (40). Because phosphorylation of KaiC is critical for negative feedback on *kaiBC* expression (10), LabA and CikA appear to act downstream of phosphorylated KaiC (40). Because the mechanisms by which LabA and/or CikA repress RpaA activation are unknown, we make the phenomenological assumption that inactive KaiC deactivates RpaA.

4. KaiC is injected into the system as fully phosphorylated hexamers. Imai et al. reported that newly synthesized KaiC is phosphorylated in vivo within 30 min (36), much faster than phosphoryla-

tion of KaiC hexamers in vitro, which takes about 6 h (12); we thus assume that newly synthesized KaiC is injected into the system as fully phosphorylated KaiC hexamers.

5. KaiA and RpaA are synthesized at constant rates. The mRNA levels of *kaiA* and *rpaA* exhibit much weaker oscillations than those of *kaiB* and *kaiC* (43). We therefore assume that *kaiA* and *rpaA* are expressed at constant rates.

6. The phosphorylation cycle in vivo is similar to that in vitro. Fig. 1*A* shows a cartoon of this model, which is described by the reactions of formulas **1–5** for the PPC together with the following reactions for the TTC and the coupling between them:

$$\tilde{\mathrm{R}} + \mathrm{X} \xrightarrow{k_a} \mathrm{R} + \mathrm{X}, \qquad \mathrm{R} + \tilde{\mathrm{X}} \xrightarrow{k_i} \tilde{\mathrm{R}} + \tilde{\mathrm{X}}, \qquad [6]$$

$$\varnothing \xrightarrow[\tau;\sigma_\tau]{\beta_c[\mathrm{R}]^4/(K^4+[\mathrm{R}]^4)} \mathrm{C}_6 + 3\mathrm{B}, \qquad [7]$$

$$\varnothing \xrightarrow{\beta_a} \mathrm{A}, \qquad \varnothing \xrightarrow{\beta_r} \tilde{\mathrm{R}}, \qquad [8]$$

$$\mathrm{R}, \tilde{\mathrm{R}}, \mathrm{A}, \mathrm{B}, \mathrm{C}_i, \mathrm{AC}_i, \mathrm{B}_x\tilde{\mathrm{C}}_i, \mathrm{A}_y\mathrm{B}_x\tilde{\mathrm{C}}_i \xrightarrow{\mu} \varnothing. \qquad [9]$$

Formula **6** models activation of inactive RpaA, $\tilde{\mathrm{R}}$, by $\mathrm{X} \in \{\mathrm{AC}_2, \ldots \mathrm{AC}_5\}$ and inactivation of active RpaA, R, by $\tilde{\mathrm{X}} \in \{\mathrm{A}_y\mathrm{B}_x\tilde{\mathrm{C}}_5 \ldots \mathrm{A}_y\mathrm{B}_x\tilde{\mathrm{C}}_2\}$ (see *SI Text*). Formula **7** models activation of *kaiBC* by RpaA, using a Hill function with coefficient 4. We assume a normally distributed delay, denoted by the double arrow, with mean $\tau = 5$ h and standard deviation $\sigma_\tau = 0.5$ h, between the activation of *kaiBC* transcription and the appearance of KaiB and KaiC protein. The length of the delay is dictated by the requirement that fresh KaiC be produced when its phosphorylation state matches that of the PPC. Formula **8** models constitutive expression of *kaiA* and *rpaA*. Formula **9** describes degradation of all species with the same rate constant μ; we ignore rhythmic KaiC degradation (36), which is not essential to produce a robust clock. In *SI Text* we show that, because of the stabilizing effect of the PPC, the clock's basic behavior is robust to variations in parameters such as the size of gene expression bursts, the width of the delay distribution, and the Hill coefficient of gene repression; there, we also discuss a more detailed model that includes cell growth and binomial partitioning upon cell division, which appreciably increases noise without changing qualitative trends. Although one can think of our model in loose terms as consisting of coupled transcriptional and post-translational oscillators, it cannot be mathematically decomposed into two separate oscillatory systems, each with its own variables, nor can the strength of the coupling between the two cycles be independently tuned. It is thus formally quite different from textbook models of coupled oscillators (44).

Fig. 4 shows the robustness of this PPC-TTC model as a function of cell volume and protein degradation rate μ. As expected, $n_{1/2}$ decreases with decreasing cell volume. Its dependence on the degradation rate, however, is markedly different from that seen with constant KaiC synthesis (Fig. 3): A PPC sustained by a TTC becomes *more* robust with increasing decay rate. If we assume that proteins are lost only through dilution, then for a bacterial volume of 1 μm^3 and a cell doubling time of 24 h (corresponding to a decay rate $\mu = 0.03$ h^{-1}), the correlation time is about 200 days, consistent with the value measured experimentally (5). If proteins are also degraded actively, increasing μ, this excellent behavior improves still further; even for $V = 0.5$ μm^3, $n_{1/2} \approx 120$ for $\mu = 0.1$ h^{-1}. This is in stark contrast to the stability of a PPC without a TTC (Fig. 3).

D. *TTC-only*: A Protein Phosphorylation Cycle Dramatically Enhances the Robustness of a Transcription–Translation Cycle. Figs. 3 and 4 show that a TTC can greatly improve the robustness of a PPC. One might thus ask whether the PPC is needed at all, or whether an adequate clock can be built with only a TTC. To address this question, we modify the PPC-TTC model (formulas **6–9**) so that it consists only of a TTC, leading to the *TTC-only* model (Fig. 1*D*):

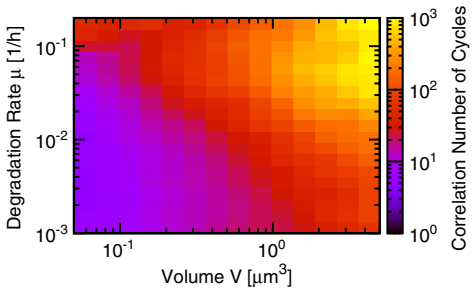

Fig. 4. *PPC-TTC* model (Fig. 1*A*). Correlation number of cycles, $n_{1/2}$, as a function of the volume V and degradation rate μ. The combination of a TTC and a PPC can generate stable circadian rhythms for a bacterial volume of $V \sim 1$ μm^3, even when the degradation rate is high (compare Fig. 3). The protein synthesis rates are varied with the degradation rates such that the average protein concentrations equal those used in vitro (see Fig. 2). For time traces of $p(t)$ and $[C](t)$, see Fig. S1.

$$\varnothing \xrightarrow[\tau;\sigma_\tau]{\beta_c[\mathrm{R}]^4/(K^4+[\mathrm{R}]^4)} \mathrm{C}, \qquad \varnothing \xrightarrow{\beta_r} \mathrm{R}, \qquad \mathrm{C}, \mathrm{R} \xrightarrow{\mu} \varnothing, \qquad [10]$$

$$\tilde{\mathrm{R}} \xrightarrow{k_a^t} \mathrm{R}, \qquad \mathrm{C} + \mathrm{R} \xrightarrow{k_i^t} \mathrm{C} + \tilde{\mathrm{R}}. \qquad [11]$$

In the simulations, we adjust not only the synthesis rate β_c but also the delay τ so that both the average concentrations and the clock period remain constant when we vary μ (see *SI Text*).

Fig. 5 shows, for a bacterial volume of 1 μm^3, the robustness of this *TTC-only* model as a function of the degradation rate, together with the results for the *PPC-TTC* model (Fig. 4) and the *PPC-in vivo* model (Fig. 3). The *TTC-only* model's behavior is the opposite of that of the *PPC-in vivo* model; the *TTC-only* model is most stable for *high* degradation rates, and its robustness falls dramatically when μ drops below 0.2 h^{-1}. The combined *PPC-TTC* model, however, is robust for all degradation rates—its correlation time interpolates between those of the *TTC-only* model for large μ and of the *PPC-in vivo* model for small μ. Importantly, the relative advantage of the combined model is greatest when $1/\mu$ is of order the oscillator period, and this is precisely the regime where physiological degradation and dilution rates for *S. elongatus* fall (36). Further, the combined oscillator does much

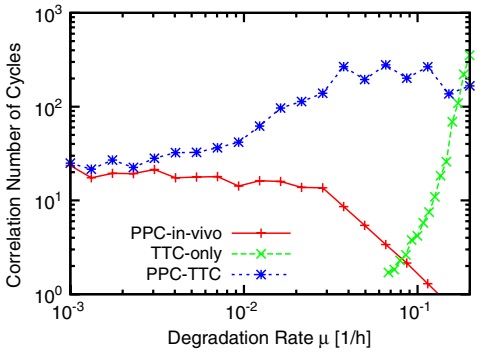

Fig. 5. Correlation number of cycles $n_{1/2}$ as a function of degradation rate μ for the *PPC-in vivo* (Fig. 1*C*), *TTC-only* (Fig. 1*D*), and *PPC-TTC* (Fig. 1*A*) models. $V = 1$ μm^3 in all models; for the TTC, $n_{1/2}$ was computed for $[\mathrm{C}](t)$ rather than for $p(t)$ (see *SI Text*). Clearly, a PPC in combination with a TTC generates robust rhythms over a wide range of degradation rates. The protein synthesis rates are varied with the degradation rates such that the average concentrations equal those used in the in vitro experiments (see Fig. 2).

better than either oscillator alone; in contrast, when two conventional phase oscillators with comparable noise levels are coupled, one expects only about a factor of two gain in $n_{1/2}$ (44).

Dilution puts a lower bound on the degradation rate, which means that a stable oscillator cannot be based on a PPC only, especially when the growth rate of the bacterium is large. The degradation rate can, on the other hand, be increased by active degradation. For high degradation rates, i.e., $\mu > 0.2\ h^{-1}$, an oscillator based only on a TTC can be sufficiently robust (Fig. 5). However, to balance these high decay rates, the protein synthesis rates have to be correspondingly large, which can be energetically costly (45). Combining a PPC with a TTC makes it possible to dramatically improve the robustness while keeping the synthesis rates the same. Although a phosphorylation cycle does not come entirely for free (46), this suggests that a PPC combined with a TTC gives the best performance-to-cost ratio.

E. The Principal Pacemaker. What drives the circadian clock, the PPC or the TTC (1)? As our analysis shows, the answer depends on the growth rate. When protein turnover is slower than the oscillation period, the clock is primarily driven by the PPC, and adding a TTC does not enhance its robustness (Fig. 5). Indeed, a TTC can generate large-amplitude oscillations in KaiC concentration only if proteins are synthesized and degraded on time scales faster than the oscillation period. At high growth rates, on the other hand, adding a PPC to a TTC does not improve stability, and the TTC is the principal driver. In this regime, the time scale for protein turnover is much faster than that for protein (de)phosphorylation; KaiC hexamers are thus typically degraded before they can complete a single phosphorylation cycle, rendering the PPC irrelevant.

To gain a deeper understanding of the transition between these two limiting cases—and in particular of the crossover regime where $1/\mu$ is of order 24 h and the gain in robustness from combining TTC and PPC is most dramatic—we introduce in *SI Text* section S2 minimal versions of the models discussed above together with two additional models designed to isolate specific modes of interaction between the two cycles (see also Fig. S2). The first of these, the *PMS-TTC* model, combines a TTC with a protein-modification sequence (PMS): the KaiC hexamers undergo a sequence of dephosphorylation steps on the PPC's inactive branch, but not a full phosphorylation cycle. The second additional model, the *UPPC-TTC* model, combines a TTC with an unsynchronized protein phosphorylation cycle (UPPC); here, each KaiC can undergo a full cycle of protein-modification steps as in the original PPC, but no KaiA is present, and synchronization through differential affinity thus cannot occur. These two models reveal two distinct mechanisms by which coupling a TTC with a PPC enhances robustness in the crossover regime (Fig. S3). The *PMS-TTC* model shows that the sequence of Poissonian protein-modification steps, an inherent property of the PPC, narrows the distribution of the delay between gene repression and gene expression, which enhances the robustness of the TTC. The *UPPC-TTC* model shows that the TTC is not only necessary to sustain a PPC at higher growth rates, as discussed above, but in fact enhances it, because the periodic synthesis of KaiC in a given phosphorylation state has a synchronizing effect on the phosphorylation cycles of the individual KaiC hexamers.

The picture that emerges from the analysis of these models is thus the following: At small μ, the PPC functions as it does in vitro, with protein synthesis and degradation playing only a minor role. As μ increases, the burden of synchronization is gradually passed from the differential affinity mechanism to periodic protein synthesis; we can still usefully think of the oscillation as driven by the PPC, but with the TTC now lending an essential helping hand. Finally, at still larger μ, $1/\mu$ becomes much larger than the oscillation period, and most hexamers do not survive long enough to complete a full phosphorylation cycle. At this point, the clock has become essentially a standard delayed negative feedback oscillator, with the twist that, unless μ is very large, the PPC helps to narrow the distribution of delay times and thus to reduce noise. Consistent with recent experiments (16), our simulations suggest that *S. elongatus* usually finds itself in the second of these regimes, in which the TTC plays an important part in synchronizing the PPC.

Discussion

The evidence is accumulating that circadian rhythms are driven by both transcription–translation and protein-modification cycles not just in cyanobacteria, but even in higher organisms (1, 47). Our analysis suggests that both cycles are required to generate stable circadian rhythms in growing, dividing cells over a wide range of conditions: Although a PPC alone must inevitably fail at high and a TTC without active degradation at low growth rates, the combined clock is robust for all growth rates. Although our *PPC-TTC* model is simplified, it does capture the essence of a coupled TTC and PPC. That is, it is built around a protein that not only undergoes a protein-modification cycle, but also regulates its own synthesis in a manner that depends on its modification state. Moreover, its qualitative behavior can be explained by the generic arguments of the preceding section, which are based on a simple comparison of the clock period with the time scales of protein modification and protein degradation. Our results should thus apply to any system that exploits both a PPC and a TTC to generate circadian rhythms.

Our combined *PPC-TTC* model is consistent with a number of experimental observations. It not only matches the average oscillations of the phosphorylation level and the total KaiC concentration in wild-type cells (Fig. S1), but also reproduces the observation that even in the presence of an excess of KaiA, the total KaiC concentration still undergoes at least a damped oscillation with a circadian period (14, 16) (see Fig. S4). Yet, because quite a few elements of the TTC have not been characterized experimentally, our model of the TTC is necessarily rather simplified and phenomenological; not surprisingly, some observations thus cannot be reproduced. For example, our model predicts that the phase of the oscillation in KaiC abundance lags behind that of the phosphorylation level by a few hours, whereas experiments seem to show that these oscillations are more in phase (12, 14). This may be due to our simplifying assumption that KaiC is produced as fully phosphorylated hexamers. Although phosphorylation of fresh KaiC has been reported to occur within 30 min (36), fragmentary evidence suggests that hexamerization is slow (48); one would then expect to detect KaiC monomers in experiments several hours before our simulations report the presence of fully functional hexamers.

In *S. elongatus*, the period of the circadian rhythm is insensitive to changes in the growth rate (49, 50). Because protein synthesis and decay rates, on the other hand, tend to vary with the growth rate (51), the question arises whether the period of the oscillator as predicted by our model is robust to such variations. In *SI Text* we show that a tenfold increase in the synthesis and degradation rates of all proteins decreases the period only by 10–20%. The reason is that the clock period is mostly determined by the intrinsic period of the PPC. The latter does not depend on the absolute protein synthesis and decay rates, although it does depend on the ratio of the concentrations of the Kai proteins (26, 33, 34). Clearly, it would be of interest to investigate how this ratio varies with the growth rate.

Finally, how could our predictions be tested experimentally? The most important testable prediction of our analysis is that the PPC requires a TTC when the growth rate is high. Kondo and coworkers have demonstrated that a PPC can function in the absence of a TTC (12). These experiments were performed under constant dark conditions, which means that the growth rate was (vanishingly) small, protein synthesis was halted, and even

protein decay was probably negligible, because the KaiC level was rather constant (12). These experiments are consistent with our predictions, but the critical test would be to increase the growth rate while avoiding any circadian regulation of *kaiBC* expression. This means that the cyanobacteria must be grown under constant light conditions. Moreover, one would need to bring *kaiBC* expression under the control of a promoter that is constitutively active. However, most promoters of *S. elongatus* (37, 43), and even many heterologous promoters from *Escherichia coli* (52), are influenced by the circadian clock. Nevertheless, a number of promoters have been reported that exhibit arrhythmic activity (43), and these might be possible candidates. A still more challenging experiment would be to express the phosphorylation cycle in the bacterium *E. coli* (53). Our analysis predicts that in growth-arrested cells, the phosphorylation cycle should be functional, whereas in normal growing *E. coli* cells, with cell doubling times of roughly 1 h, the oscillations should cease to exist.

Methods

The simulations were performed using the algorithm of ref. 35, and $n_{1/2}$ was computed from the decay of the correlation function of $p(t)$, except for the *TTC-only* model, for which we used $[C](t)$; our estimates for $n_{1/2}$ are typically accurate to within 15–20% (see *SI Text*).

ACKNOWLEDGMENTS. We thank Tom Shimizu for critically reading the manuscript. This work was supported in part by FOM, which is financially supported by the "Nederlandse Organisatie voor Wetenschappelijk Onderzoek" (D.Z. and P.R.t.W.) and by NSF Grant PHY05-51164 to the Kavli Institute for Theoretical Physics (to D.K.L.).

1. Johnson CH, Egli M, Stewart PL (2008) Structural insights into a circadian oscillator. *Science* 322:697–701.
2. Elowitz MB, Levine AJ, Siggia ED, Swain PS (2002) Stochastic gene expression in a single cell. *Science* 297:1183–1186.
3. Liu C, Weaver DR, Strogatz SH, Reppert SM (1997) Cellular construction of a circadian clock: Period determination in the suprachiasmatic nuclei. *Cell* 91:855–860.
4. Yamaguchi S, et al. (2003) Synchronization of cellular clocks in the suprachiasmatic nucleus. *Science* 302:1408–1412.
5. Mihalcescu I, Hsing W, Leibler S (2004) Resilient circadian oscillator revealed in individual cyanobacteria. *Nature* 430:81–85.
6. Amdaoud M, Vallade M, Weiss-Schaber C, Mihalcescu I (2007) Cyanobacterial clock, a stable phase oscillator with negligible intercellular coupling. *Proc Natl Acad Sci USA* 104:7051–7056.
7. Ishiura M, et al. (1998) Expression of a gene cluster *kaiABC* as a circadian feedback process in cyanobacteria. *Science* 281:1519–1523.
8. Xu Y, Mori T, Johnson CH (2000) Circadian clock-protein expression in cyanobacteria: Rhythms and phase setting. *EMBO J* 19:3349–3357.
9. Nakahira Y, et al. (2004) Global gene repression by KaiC as a master process of prokaryotic circadian system. *Proc Natl Acad Sci USA* 101:881–885.
10. Nishiwaki T, et al. (2004) Role of KaiC phosphorylation in the circadian clock system of synechococcus elongatus pcc 7942. *Proc Natl Acad Sci USA* 101:13927–13932.
11. Kageyama H, Kondo T, Iwasaki H (2003) Circadian formation of clock protein complexes by KaiA, KaiB, KaiC, and SasA in cyanobacteria. *J Biol Chem* 278:2388–2395.
12. Tomita J, Nakajima M, Kondo T, Iwasaki H (2005) No transcription-translation feedback in circadian rhythm of KaiC phosphorylation. *Science* 307:251–254.
13. Nakajima M, et al. (2005) Reconstitution of circadian oscillation of cyanobacterial KaiC phosphorylation in vitro. *Science* 308:414–415.
14. Kitayama Y, Nishiwaki T, Terauchi K, Kondo T (2008) Dual KaiC-based oscillations constitute the circadian system of cyanobacteria. *Genes Dev* 22:1513–1521.
15. Ito H, et al. (2007) Autonomous synchronization of the circadian KaiC phosphorylation rhythm. *Nat Struct Mol Biol* 14:1084–1088.
16. Qin X, Byrne M, Xu Y, Mori T, Johnson CH (2010) Coupling of a core post-translational pacemaker to a slave transcription/translation feedback loop in a circadian system. *PLoS Biol* 8:e1000394.
17. Nishiwaki T, et al. (2007) A sequential program of dual phosphorylation of KaiC as a basis for circadian rhythm in cyanobacteria. *EMBO J* 26:4029–4037.
18. Rust MJ, Markson JS, Lane WS, Fisher DS, O'Shea EK (2007) Ordered phosphorylation governs oscillation of a three-protein circadian clock. *Science* 318:809–812.
19. Iwasaki H, Nishiwaki T, Kitayama Y, Nakajima M, Kondo T (2002) KaiA-stimulated KaiC phosphorylation in circadian timing loops in cyanobacteria. *Proc Natl Acad Sci USA* 99:15788–15793.
20. Xu Y, Mori T, Johnson CH (2003) Cyanobacterial circadian clockwork: Roles of KaiA, KaiB and the *kaiBC* promoter in regulating KaiC. *EMBO J* 22:2117–2126.
21. Kitayama Y, Iwasaki H, Nishiwaki T, Kondo T (2003) KaiB functions as an attenuator of KaiC phosphorylation in the cyanobacterial circadian clock system. *EMBO J* 22:2127–2134.
22. Williams SB, Vakonakis I, Golden SS, LiWang AC (2002) Structure and function from the circadian clock protein KaiA of *Synechococcus elongatus*: A potential clock input mechanism. *Proc Natl Acad Sci USA* 99:15357–15362.
23. Takigawa-Imamura H, Mochizuki A (2006) Predicting regulation of the phosphorylation cycle of KaiC clock protein using mathematical analysis. *J Biol Rhythm* 21:405–416.
24. Emberly E, Wingreen NS (2006) Hourglass model for a protein-based circadian oscillator. *Phys Rev Lett* 96:038303.
25. Mehra A, et al. (2006) Circadian rhythmicity by autocatalysis. *PLoS Comput Biol* 2:e96.
26. van Zon JS, Lubensky DK, Altena PRH, ten Wolde PR (2007) An allosteric model of circadian KaiC phosphorylation. *Proc Natl Acad Sci USA* 104:7420–7425.
27. Clodong S, et al. (2007) Functioning and robustness of a bacterial circadian clock. *Mol Syst Biol* 3:90.
28. Mori T, et al. (2007) Elucidating the ticking of an in vitro circadian clockwork. *PLoS Biol* 5:e93.
29. Miyoshi F, Nakayama Y, Kaizu K, Iwasaki H, Tomita M (2007) A mathematical model for the Kai-protein-based chemical oscillator and clock gene expression rhythms in cyanobacteria. *J Biol Rhythm* 22:69–80.
30. Yoda M, Eguchi K, Terada TP, Sasai M (2007) Monomer-shuffling and allosteric transition in KaiC circadian oscillation. *PLoS One* 2:e408.
31. Eguchi K, Yoda M, Terada TP, Sasai M (2008) Mechanism of robust circadian oscillation of KaiC phosphorylation in vitro. *Biophys J* 95:1773–1784.
32. Markson JS, O'Shea EK (2009) The molecular clockwork of a protein-based circadian oscillator. *FEBS Lett* 583:3938–3947.
33. Nakajima M, Ito H, Kondo T (2010) In vitro regulation of circadian phosphorylation rhythm of cyanobacterial clock protein KaiC by KaiA and KaiB. *FEBS Lett* 584(5): 898–902.
34. Kageyama H, et al. (2006) Cyanobacterial circadian pacemaker: Kai protein complex dynamics in the KaiC phosphorylation cycle in vitro. *Mol Cell* 23:161–171.
35. Gillespie DT (1977) Exact stochastic simulation of coupled chemical reactions. *J Phys Chem* 81:2340–2361.
36. Imai K, Nishiwaki T, Kondo T, Iwasaki H (2004) Circadian rhythms in the synthesis and degradation of a master clock protein KaiC in cyanobacteria. *J Biol Chem* 279:36534–36539.
37. Vijayan V, Zuzow R, O'Shea EK (2009) Oscillations in supercoiling drive circadian gene expression in cyanobacteria. *Proc Natl Acad Sci USA* 106:22564–22568.
38. Smith RM, Williams SB (2006) Circadian rhythms in gene transcription imparted by chromosome compaction in the cyanobacterium *Synechococcus elongatus*. *Proc Natl Acad Sci USA* 103:8564–8569.
39. Woelfle MA, Xu Y, Qin X, Johnson CH (2007) Circadian rhythms of superhelical status of DNA in cyanobacteria. *Proc Natl Acad Sci USA* 104:18819–18824.
40. Taniguchi Y, Takai N, Katayama M, Kondo T, Oyama T (2010) Three major output pathways from the KaiABC-based oscillator cooperate to generate robust circadian *kaiBC* expression in cyanobacteria. *Proc Natl Acad Sci USA* 107:3263–3268.
41. Taniguchi Y, et al. (2007) *labA*: A novel gene required for negative feedback regulation of the cyanobacterial circadian clock protein KaiC. *Genes Dev* 21:60–70.
42. Takai N, et al. (2006) A KaiC-associating SasA-RpaA two-component regulatory system as a major circadian timing mediator in cyanobacteria. *Proc Natl Acad Sci USA* 103:12109–12114.
43. Ito H, et al. (2009) Cyanobacterial daily life with Kai-based circadian and diurnal genome-wide transcriptional control in *Synechococcus elongatus*. *Proc Natl Acad Sci USA* 106:14168–14173.
44. Pikovsky A, Rosenblum M, Kurths J (2001) *Synchronization, A Universal Concept in Nonlinear Sciences* (Cambridge Univ Press, Cambridge, UK).
45. Dekel E, Alon U (2005) Optimality and evolutionary tuning of the expression level of a protein. *Nature* 436:588–592.
46. Terauchi K, et al. (2007) ATPase activity of KaiC determines the basic timing for circadian clock of cyanobacteria. *Proc Natl Acad Sci USA* 104:16377–16381.
47. Merrow M, Roenneberg T (2007) Circadian clock: Time for a phase shift of ideas? *Curr Biol* 17:R636–638.
48. Mori T, et al. (2002) Circadian clock protein KaiC forms ATP-dependent hexameric rings and binds DNA. *Proc Natl Acad Sci USA* 99:17203–17208.
49. Mori T, Binder B, Johnson CH (1996) Circadian gating of cell division in cyanobacteria growing with average doubling times of less than 24 hours. *Proc Natl Acad Sci USA* 93:10183–10188.
50. Kondo T, et al. (1997) Circadian rhythms in rapidly dividing cyanobacteria. *Science* 275:224–227.
51. Klumpp S, Zhang Z, Hwa T (2009) Growth rate-dependent global effects on gene expression in bacteria. *Cell* 139:1366–1375.
52. Ditty JL, Williams SB, Golden SS (2003) A cyanobacterial circadian timing mechanism. *Annu Rev Genet* 37:513–543.
53. Tozaki H, Kobe T, Aihara K, Iwasaki H (2008) An attempt to reveal a role of a transcription/translation feedback loop in the cyanobacterial kaic protein-based circadian system by using a semi-synthetic method. *Int J Bioinform Res Appl* 4:435–444.

Supporting Information

Zwicker et al. 10.1073/pnas.1007613107

SI Text

S1. The Models. ***S1.1. PPC-in vitro model: A PPC with constant protein copy numbers.*** Fig. 1*B* of the main text shows a cartoon of the *PPC-in vitro* model. In this model of the protein phosphorylation cycle (PPC) the total concentration of each Kai protein is constant. The model is described by reactions **1**–**5** of the main text, which we repeat here:

$$\mathrm{C}_i \underset{b_i}{\overset{f_i}{\rightleftarrows}} \tilde{\mathrm{C}}_i, \qquad \mathrm{C}_i + \mathrm{A} + \underset{k_i^{\mathrm{Ab}}}{\overset{k_i^{\mathrm{Af}}}{\rightleftarrows}} \mathrm{AC}_i \overset{k_{\mathrm{pf}}}{\rightarrow} \mathrm{C}_{i+1} + \mathrm{A}, \qquad \textbf{[S1]}$$

$$\tilde{\mathrm{C}}_i + \mathrm{B} \underset{\tilde{k}_i^{\mathrm{Bb}}}{\overset{2\tilde{k}_i^{\mathrm{Bf}}}{\rightleftarrows}} \mathrm{B}\tilde{\mathrm{C}}_i, \qquad \mathrm{B}\tilde{\mathrm{C}}_i + \mathrm{B} \underset{2\tilde{k}_i^{\mathrm{Bb}}}{\overset{\tilde{k}_i^{\mathrm{Bf}}}{\rightleftarrows}} \mathrm{B}_2\tilde{\mathrm{C}}_i, \qquad \textbf{[S2]}$$

$$\mathrm{B}_x\tilde{\mathrm{C}}_i + \mathrm{A} \underset{\tilde{k}_i^{\mathrm{Ab}}}{\overset{x\tilde{k}_i^{\mathrm{Af}}}{\rightleftarrows}} \mathrm{AB}_x\tilde{\mathrm{C}}_i, \qquad \mathrm{AB}_2\tilde{\mathrm{C}}_i + \mathrm{A} \underset{2\tilde{k}_i^{\mathrm{Ab}}}{\overset{\tilde{k}_i^{\mathrm{Af}}}{\rightleftarrows}} \mathrm{A}_2\mathrm{B}_2\tilde{\mathrm{C}}_i, \qquad \textbf{[S3]}$$

$$\mathrm{C}_i \underset{k_{\mathrm{dps}}}{\overset{k_{\mathrm{ps}}}{\rightleftarrows}} \mathrm{C}_{i+1}, \qquad \tilde{\mathrm{C}}_i \underset{\tilde{k}_{\mathrm{dps}}}{\overset{\tilde{k}_{\mathrm{ps}}}{\rightleftarrows}} \tilde{\mathrm{C}}_{i+1}, \qquad \textbf{[S4]}$$

$$\mathrm{B}_x\tilde{\mathrm{C}}_i \underset{\tilde{k}_{\mathrm{dps}}}{\overset{\tilde{k}_{\mathrm{ps}}}{\rightleftarrows}} \mathrm{B}_x\tilde{\mathrm{C}}_{i+1}, \qquad \mathrm{A}_y\mathrm{B}_x\tilde{\mathrm{C}}_i \underset{\tilde{k}_{\mathrm{dps}}}{\overset{\tilde{k}_{\mathrm{ps}}}{\rightleftarrows}} \mathrm{A}_y\mathrm{B}_x\tilde{\mathrm{C}}_{i+1}. \qquad \textbf{[S5]}$$

Here, C_i denotes a KaiC hexamer in the active conformational state, in which the number i of phosphorylated monomers tends to increase, and $\tilde{\mathrm{C}}_i$ denotes a KaiC hexamer in the inactive conformational state in which i tends to decrease; A denotes a KaiA dimer, and B denotes a KaiB dimer. The reactions $\mathrm{C}_i \rightleftarrows \tilde{\mathrm{C}}_i$ in **S1** model the conformational transitions between active and inactive KaiC; the second set of reactions in **S1** describe phosphorylation of active KaiC that is stimulated by KaiA; the reactions in **S2** model the binding of KaiB to inactive KaiC and those in **S3** model the sequestration of KaiA by inactive KaiC that is bound to KaiB; note that an inactive KaiC hexamer can bind up to two KaiA dimers; the reactions in **S4** and **S5** model spontaneous phosphorylation and dephosphorylation of active and inactive KaiC. For a more detailed discussion of the model, we refer to ref. 1.

We study this model, as well as the other stochastic models discussed below, using kinetic Monte Carlo simulations of the chemical master equation (2). In our simulations, we vary the reaction volume, but keep the concentrations of the Kai proteins constant at levels comparable to those used in the in vitro experiments (3, 4). Fig. S1*A* shows two time traces of the phosphorylation level $p(t)$, defined as the fraction of monomers that is phosphorylated, for two different volumes, whereas Fig. 2 of the main text shows the correlation number of cycles, $n_{1/2}$, as a function of the volume; for a discussion of how $n_{1/2}$ is computed, see section S7.

Comparing the robustness with in vivo measurements. Fig. 2 of the main text shows that $n_{1/2}$ increases with the volume. To compare our predictions with the experimental results obtained in vivo (5), we have to verify that the concentrations of the Kai proteins in vitro/in silico are similar to those in vivo, because the behavior of the phosphorylation cycle depends on the concentrations of the Kai proteins (3, 4). The copy number of KaiC monomers in vivo has been measured (6) to be around 10,000, corresponding to roughly 1,000 KaiC hexamers, which, assuming that the bacterium is roughly 1 cubic micron, corresponds to a KaiC hexamer concentration of about 1 μM, comparable to the KaiC hexamer concentration in vitro (3, 4). It thus seems meaningful to compare the predictions of Fig. 2 of the main text with experiment. Our model predicts that for a bacterial volume of 1 cubic micron, the phosphorylation cycle is highly robust, with $n_{1/2} \approx 200$, in agreement with what has been measured experimentally in vivo, which is $n_{1/2} = 166 \pm 100$ days (5). However, the number of KaiA monomers in vivo has been measured to be on the order of 250–500 monomers (6), corresponding to 125–250 KaiA dimers. This means that in vivo the concentration ratio of KaiA dimers to KaiC hexamers is about 1:6, which is lower than the corresponding ratio in the test tube, which is 1:1 (3). In fact, for the in vivo concentration ratio of KaiA to KaiC, the in vitro system does not exhibit macroscopic phosphorylation oscillations (3, 4). It has therefore been suggested that in vivo the oscillations are confined to a small subcellular domain from which some KaiB and KaiC molecules are excluded (6), allowing the reactions to proceed at roughly the in vitro ratio; here, we adopt this hypothesis and assume that the Kai proteins are found in the physiologically relevant reaction volume in proportions comparable to those used in the in vitro experiments. If we take this volume to be a third of the total bacterial volume, i.e., $V \sim 0.3\ \mu\mathrm{m}^3$—small enough that the measured number of KaiA molecules is more than adequate to give the in vitro KaiA dimer concentration of 0.58 μM (3, 4)—then our model predicts that the phosphorylation cycle has a correlation time of roughly 75 days. This would still be consistent with the value measured experimentally (5), in contrast to the models proposed by Eguchi et al. (7) and Rust et al. (8) (see section S5). Our model thus predicts that the phosphorylation cycle is highly robust against the intrinsic noise arising from the stochastic nature of the phosphorylation reactions and the physical interactions between the Kai proteins.

S1.2. PPC-in vivo model: A PPC with constant protein synthesis and degradation rates. In the main text, we also discuss the performance of a model that includes not only a PPC, but also synthesis and degradation of the Kai proteins; we call this model the *PPC-in vivo* model. This model is described in reactions **S1**–**S5** plus the following reactions for the synthesis and degradation of the Kai proteins:

$$\varnothing \overset{\beta_{\mathrm{c}}}{\rightarrow} \mathrm{C}_6 + 3\mathrm{B}, \qquad \varnothing \overset{\beta_{\mathrm{a}}}{\rightarrow} \mathrm{A}, \qquad \textbf{[S6]}$$

$$\mathrm{A}, \mathrm{B}, \mathrm{C}_i, \mathrm{AC}_i, \mathrm{B}_x\tilde{\mathrm{C}}_i, \mathrm{A}_y\mathrm{B}_x\tilde{\mathrm{C}}_i \overset{\mu}{\rightarrow} \varnothing. \qquad \textbf{[S7]}$$

As explained in the main text, we assume that fresh KaiC is injected into the system as fully phosphorylated hexamers because phosphorylation of fresh KaiC proteins has been reported to be fast, i.e., occurring within 30 min (9). However, the precise choice for the phosphoform of fresh KaiC is not so important in this model; it does not affect the robustness of this model. Because the KaiB and KaiC proteins are both products of the *kaiBC* operon, we choose to model the production of both proteins as a single reaction. We note that while in the model with the transcription–translation cycle, discussed in section S1.4, the delay

in the synthesis reactions is critical, in the above model, where the Kai proteins are produced with rates that are constant in time, a delay would have no effect; the synthesis reactions are therefore modeled as simple, Poissonian birth reactions. Fig. S1*B* shows time traces for the phosphorylation level $p(t)$ for three different degradation rates.

S1.3. Deterministic PPC-in vivo model. To verify that the disappearance of oscillations as the degradation rate is increased is not a purely stochastic effect, we consider the model of **S1**–**S7** in the deterministic limit of infinite volume and protein number. In this limit, the concentrations of the different proteins evolve according to deterministic rate equations. We make two further simplifying assumptions: First, we replace the two-step binding of KaiB to $\tilde{C}_i$ with a trimolecular reaction that turns $\tilde{C}_i$ directly into $B_2\tilde{C}_i$, and making a similar change for binding of KaiA to the inactive branch. Second, we assume that binding and unbinding reactions are fast enough that they are effectively in steady state and thus explicitly keep track only of the concentrations of the various KaiC species; the concentrations of free KaiA and KaiB can then be inferred from conservation laws. The dynamical equations are then essentially the same as those given in equations 44–47 of our previous publication (1), with the addition of a linear decay term with rate μ for each species and of synthesis of C_6 with rate β_c:

$$\frac{d[C_i]_T}{dt} = \sigma_{i-1}^{ps}[C_{i-1}]_T + \sigma_{i+1}^{dps}[C_{i+1}]_T - (\sigma_i^{ps} + \sigma_i^{dps})[C_i]_T - \sigma_i^{Ff}[C_i]_T + \sigma_i^{Fb}[\tilde{C}_i], + \beta_c\delta_{i,6} - \mu[C_i]_T, \quad \textbf{[S8]}$$

$$\frac{d[\tilde{C}_i]}{dt} = \tilde{k}_{ps}[\tilde{C}_{i-1}] + \tilde{k}_{dps}[\tilde{C}_{i+1}] - (\tilde{k}_{ps} + \tilde{k}_{dps})[\tilde{C}_i] + \sigma_i^{Ff}[C_i]_T - \sigma_i^{Fb}[\tilde{C}_i] - \tilde{\kappa}_i^{Bf}([B])_T - 2\Sigma_i[B_2\tilde{C}_i]_T)^2[\tilde{C}_i] + \frac{\tilde{\kappa}_i^{Bb}\tilde{K}_i[B_2\tilde{C}_i]_T}{\tilde{K}_i + [A]^2} - \mu[\tilde{C}_i], \quad \textbf{[S9]}$$

$$\frac{d[B_2\tilde{C}_i]_T}{dt} = \tilde{k}_{ps}[B_2\tilde{C}_{i-1}]_T + \tilde{k}_{dps}[B_2\tilde{C}_{+1}]_T - (\tilde{k}_{ps} + \tilde{k}_{dps})[B_2\tilde{C}_i]_T + \tilde{\kappa}_i^{Bf}([B]_T - 2\Sigma_i[B_2\tilde{C}_i]_T)^2[\tilde{C}_i] - \frac{\tilde{\kappa}_i^{Bb}\tilde{K}_i[B_2\tilde{C}_i]_T}{\tilde{K}_i + [A]^2} - \mu[B_2\tilde{C}_i]_T, \quad \textbf{[S10]}$$

where the concentration of free KaiA, [A], is given by

$$[A] + \sum_{i=0}^{N}\frac{[A][C_i]_T}{K_i + [A]} + 2\sum_{i=0}^{N}\frac{[A]^2[B_2\tilde{C}_i]_T}{\tilde{K}_i^2 + [A]^2} - [A]_T = 0. \quad \textbf{[S11]}$$

Here $[C_i]_T$ is the total concentration of KaiC hexamers with i phosphorylated monomers in the active state, whether or not complexed with KaiA, i.e., $[C_i]_T = [C_i] + [AC_i]$; $[B_2\tilde{C}_i]_T$ is defined similarly. The effective rate constants appearing in these equations depend on the concentration [A] of free KaiA and are defined in terms of the more microscopic rate constants as follows: The effective (de)phosphorylation rates on the active branch are $\sigma_i^{ps} = (k_{ps}K_i + k_{pf}[A])/(K_i + [A])$ and $\sigma_i^{dps} = K_i k_{dps}/(K_i + [A])$. The effective flipping rates are given by $\sigma_i^{Ff} = f_i K_i/(K_i + [A])$ and $\sigma_i^{Fb} = b_i$, where f_i and b_i are the forward and backward flipping rates. The parameters $\tilde{\kappa}_i^{Bf}$ and $\tilde{\kappa}_i^{Bb}$ differ from $\tilde{k}_i^{Bf}$ and $\tilde{k}_i^{Bb}$, respectively, in that the κ's are rate constants for trimolecular reactions, which are broken down into two successive bimolecular reactions in the stochastic simulations. The dissociation constants K_i satisfy $K_i = k_i^{Ab}/k_i^{Af}$; the $\tilde{K}_i$ could be defined similarly in terms of forward and backward rates for KaiA binding to the inactive branch, but (just as with $\tilde{\kappa}_i^{Bf}$ and $\tilde{\kappa}_i^{Bb}$) these rates would differ from those used in the stochastic simulations, so we choose instead to quote the dissociation constants directly. Following ref. 1, we choose values for the new parameters associated with trimolecular interactions such that time dependence of $p(t)$ matches the average behavior of the stochastic model.

To determine where oscillations disappear as μ is increased, we analyzed these equations using the XPPAUT implementation of the AUTO continuation package (10). We found that, for the parameter values given in Table S1, the system undergoes a supercritical Hopf bifurcation at $\mu = 0.0621\ h^{-1}$, as noted in the main text.

S1.4. PPC-TTC model: The PPC and TTC combined. The *PPC-TTC* model of the main text consists of a PPC, a transcription–translation cycle (TTC), and a pathway that couples these two cycles. This model is described by the reactions of **S1**–**S5** for the PPC, together with the following reactions for the TTC and the coupling between them:

$$\tilde{R} + X \xrightarrow{k_a} R + X, \qquad R + \tilde{X} \xrightarrow{k_i} \tilde{R} + \tilde{X}, \quad \textbf{[S12]}$$

$$\varnothing \xrightarrow[\tau\pm\sigma_\tau]{\beta_c[R]^n/(K^n+[R]^n)} C_6 + 3B, \qquad \varnothing \xrightarrow{\beta_a} A, \qquad \varnothing \xrightarrow{\beta_r} \tilde{R}, \quad \textbf{[S13]}$$

$$R,\tilde{R},A,B,C_i,AC_i,B_xC_i,A_yB_x\tilde{C}_i \xrightarrow{\mu} \varnothing. \quad \textbf{[S14]}$$

Here, R and $\tilde{R}$ denote the RpaA protein in its active and its inactive form, respectively, whereas n is the Hill coefficient of gene repression; its baseline value is $n = 4$, but in section S4.3 we study the effect of varying n. The X and $\tilde{X}$ in **S12** denote any of the phosphoforms of KaiC that mediate the activation and repression of RpaA, respectively; in section S4.1, we discuss the dependence of the results on precisely which phosphoforms are chosen to activate and repress RpaA, respectively. The double arrow indicates a reaction with a Gaussian distributed delay with mean τ and variance σ_τ. We thus assume that *kaiBC* expression is activated by RpaA, where the activity of RpaA is modulated by the PPC. In contrast, the expression of KaiA, KaiB, and RpaA is assumed to occur constitutively. Fig. S1*C* shows time traces for the phosphorylation level $p(t)$ and total KaiC concentration $[C]_T(t)$ for $V = 1\ \mu m^3$ and $\mu = 0.03\ h^{-1}$ (solid lines) and $\mu = 0.1\ h^{-1}$ (dotted lines), respectively.

S1.5. TTC-only model. The *TTC-only* model is given by the following reactions:

$$\varnothing \xrightarrow[\tau;\sigma_\tau]{\beta_c[R]^4/(K^4+[R]^4)} C, \qquad \varnothing \xrightarrow{\beta_r} R, \qquad C,R \xrightarrow{\mu} \varnothing, \quad \textbf{[S15]}$$

$$\tilde{R} \xrightarrow{k_r^t} R, \qquad C + R \xrightarrow{k_i^t} C + \tilde{R}. \quad \textbf{[S16]}$$

In the simulations, we adjust the delay τ and the synthesis rate β_c for each choice of the degradation rate μ such that the oscillation period is 24 h and the average KaiC concentration is comparable to that of the other models considered so far. Fig. S1*D* shows time traces for the concentrations of KaiC and active RpaA, respectively. In section S2 we discuss the simplest possible TTC model, namely one in which KaiC directly represses its own synthesis; this gave very similar results.

S1.6. Parameters. Table S1 gives the values of the parameters used in the stochastic simulations based on the kinetic Monte Carlo algorithm developed by Gillespie (2). Unless otherwise noted,

we choose the total concentrations of the Kai proteins to match common conditions for the in vitro reaction system (3, 4): $[A]_T = 0.58$ μM, $[B]_T = 1.75$ μM, and $[C]_T = 0.58$ μM.

S2. A Simplified Description Provides Insight into the *PPC-TTC* Model's Robustness. To elucidate why a clock built upon a TTC and a PPC is robust across a range of protein turnover rates, we study minimal versions of the models discussed above. We also introduce two new models, the *PMS-TTC* model and the *UPPC-TTC* model, that represent intermediate cases between the extremes of the coupled *PPC-TTC* model on the one hand and the separate *PPC-in vivo* and *TTC-only* models on the other. Cartoons of these new models are shown in Fig. S2 *A–D*. Below, we first briefly describe the different models and then use them to explain why a PPC enhances the robustness of a TTC, and vice versa. Throughout this section, we refer to the more realistic models introduced in the main text, and discussed in the preceding section, as *full* models, while the simplified versions considered in this section are called *minimal* models. The parameters of the minimal models are shown in Table S1.

Minimal PPC-in vivo model. In the minimal *PPC-in vivo* model, the binding of KaiB to KaiC has been integrated out and intermediate conformational transitions between active and inactive KaiC are disallowed. The model is described by the following reactions:

$$\mathrm{C}_6 \xrightarrow{f_6} \tilde{\mathrm{C}}_6, \qquad \tilde{\mathrm{C}}_0 \xrightarrow{b_0} \mathrm{C}_0, \qquad \mathrm{C}_i + \mathrm{A} \underset{k_i^{\mathrm{Ab}}}{\overset{k_i^{\mathrm{Af}}}{\rightleftarrows}} \mathrm{AC}_i \xrightarrow{k_{\mathrm{pf}}} \mathrm{C}_{i+1} + \mathrm{A}, \qquad \text{[S17]}$$

$$\tilde{\mathrm{C}}_i + \mathrm{A} \underset{\tilde{k}_i^{\mathrm{Ab}}}{\overset{2\tilde{k}_i^{\mathrm{Af}}}{\rightleftarrows}} \mathrm{A}\tilde{\mathrm{C}}_i, \qquad \mathrm{A}\tilde{\mathrm{C}}_i + \mathrm{A} \underset{2\tilde{k}_i^{\mathrm{Ab}}}{\overset{\tilde{k}_i^{\mathrm{Af}}}{\rightleftarrows}} \mathrm{A}_2\tilde{\mathrm{C}}_i, \qquad \text{[S18]}$$

$$\mathrm{C}_i \underset{k_{\mathrm{dps}}}{\overset{k_{\mathrm{ps}}}{\rightleftarrows}} \mathrm{C}_{i+1}, \qquad \tilde{\mathrm{C}}_i \underset{\tilde{k}_{\mathrm{dps}}}{\overset{\tilde{k}_{\mathrm{ps}}}{\rightleftarrows}} \tilde{\mathrm{C}}_{i+1}, \qquad \mathrm{A}_y\tilde{\mathrm{C}}_i \underset{\tilde{k}_{\mathrm{dps}}}{\overset{\tilde{k}_{\mathrm{ps}}}{\rightleftarrows}} \mathrm{A}_y\tilde{\mathrm{C}}_{i+1}, \qquad \text{[S19]}$$

$$\varnothing \xrightarrow{\beta_{\mathrm{c}}} \mathrm{C}_6, \qquad \varnothing \xrightarrow{\beta_{\mathrm{a}}} \mathrm{A}, \qquad \mathrm{A}, \mathrm{C}_i, \mathrm{AC}_i, \mathrm{A}_y\tilde{\mathrm{C}}_i \xrightarrow{\mu} \varnothing. \qquad \text{[S20]}$$

These equations give a generic description of a protein modification cycle that is synchronized via the mechanism of differential affinity (1), in which KaiA sequestration synchronizes the phosphorylation cycles of different KaiC hexamers. The solid red line of Fig. S2*E* shows the correlation number of cycles, $n_{1/2}$, as a function of the degradation rate μ for $V = 1$ μm^3 for this minimal *PPC-in vivo* model; when μ is varied, the protein synthesis rates are adjusted such that the average protein concentrations are unchanged. The minimal model's behavior is not only qualitatively, but also quantitatively very similar to that of the full *PPC-in-vivo* model (Fig. 5 of main text); in particular, the PPC alone is stable only at low protein degradation rates.

Minimal TTC-only model. The simplest and most generic TTC model is one in which KaiC directly represses its own synthesis (with a delay, indicated by a double arrow as in the main text):

$$\varnothing \xrightarrow[\tau;\sigma_\tau]{\beta_{\mathrm{c}}\mathrm{K}^4/(\mathrm{K}^4+[\mathrm{C}]^4)} \mathrm{C}, \qquad \mathrm{C} \xrightarrow{\mu} \varnothing. \qquad \text{[S21]}$$

It can be seen that in comparison to the *TTC-only* model of the main text, here RpaA has been integrated out. The green line of Fig. S2*E* shows $n_{1/2}$ as a function of μ for $V = 1$ μm^3; when μ is varied, both the protein synthesis rate β_{c} and the delay in protein synthesis τ are adjusted such that the average KaiC concentration and the oscillation period remain constant. The minimal model behaves very similarly to the full *TTC-only* model discussed in the main text (see Fig. 5), showing robust oscillations only for high protein turnover rates.

Minimal PPC-TTC model. The PPC of the minimal *PPC-TTC* model is given by the minimal PPC described above (**S17–S20**). In the full *PPC-TTC* model, the active KaiC phosphoforms activate RpaA and thereby stimulate KaiC synthesis, whereas the inactive KaiC phosphoforms deactivate RpaA and thereby repress KaiC synthesis. In the minimal *PPC-TTC* model, we have integrated out RpaA. Moreover, we assume that only the inactive KaiC phosphoforms regulate, i.e., repress, KaiC synthesis. This yields the following synthesis and decay reactions:

$$\varnothing \xrightarrow[\tau;\sigma_\tau]{\beta_{\mathrm{c}}\mathrm{K}^4/(\mathrm{K}^4+[\mathrm{R}]^4)} \mathrm{C}_6, \qquad \varnothing \xrightarrow{\beta_{\mathrm{a}}} \mathrm{A}, \qquad \text{[S22]}$$

$$\mathrm{A}, \mathrm{C}_i, \mathrm{AC}_i, \mathrm{A}_y\tilde{\mathrm{C}}_i \xrightarrow{\mu} \varnothing. \qquad \text{[S23]}$$

Here, $[\mathrm{R}] = \sum_{i=0}^{6}(\tilde{\mathrm{C}}_i + [\mathrm{A}\tilde{\mathrm{C}}_i] + [\mathrm{A}_2\tilde{\mathrm{C}}_i])$ is the total concentration of all the KaiC phosphoforms that are in the inactive state. The blue line of Fig. S2*E* shows the correlation number of cycles $n_{1/2}$ as a function of the degradation rate μ for $V = 1$ μm^3 for this model. As μ is varied, the protein synthesis rates are adjusted to keep the average protein concentrations constant, but it turns out not to be necessary to change the delay τ in protein synthesis, because the period of the clock is dictated primarily by the PPC (see section S6 for a more detailed discussion). As expected, the behavior of the minimal *PPC-TTC* model is similar to that of the full *PPC-TTC* model discussed in the main text; the clock is robust not only in the limiting regimes of low and high protein turnover rates, but also in the biologically relevant crossover regime.

Minimal PMS-TTC model. This model is meant to capture one possible effect on the TTC of coupling it to the PPC: Rather than disappearing only through first-order degradation at a rate μ, as they do in the *TTC-only* model, the KaiC forms that repress transcription can also, when a PPC is present, be eliminated by their advance through KaiC's phosphorylation cycle, which must eventually turn repressing hexamers $\tilde{\mathrm{C}}_i$ on the inactive branch into active hexamers C_i that do not affect transcription. Moreover, because progress through the phosphorylation cycle involves a sequence of first-order steps, the distribution of times for repressors to disappear via this new route will be narrower than the distribution of degradation times, which should in turn increase the clock's robustness. To elucidate these effects, the *PMS-TTC* model combines a TTC with a protein modification sequence (PMS): The proteins do not undergo a full cycle of protein modification steps, as in the original PPC, but a half cycle, during which they progress through a *sequence* of repressive KaiC phosphoforms before being converted into the C_0 form that cannot regulate transcription. The model is described by the following reactions:

$$\mathrm{C}_6 \xrightarrow{f_6} \tilde{\mathrm{C}}_6, \qquad \tilde{\mathrm{C}}_0 \xrightarrow{b_0} \mathrm{C}_0, \qquad \text{[S24]}$$

$$\tilde{\mathrm{C}}_i \xrightarrow{\tilde{k}_{\mathrm{dps}}} \tilde{\mathrm{C}}_{i-1}, \qquad \text{[S25]}$$

$$\varnothing \xrightarrow[\tau;\sigma_\tau]{\beta_{\mathrm{c}}\mathrm{K}^4/(\mathrm{K}^4+[\mathrm{R}]^4)} \mathrm{C}_6, \qquad \mathrm{C}_6, \mathrm{C}_0, \tilde{\mathrm{C}}_i \xrightarrow{\mu} \varnothing. \qquad \text{[S26]}$$

Here, $[\mathrm{R}] = \sum_{i=0}^{6}[\tilde{\mathrm{C}}]_i$ is the total concentration of inactive KaiC, which represses *kaiC*. Note that, in order to maintain as close a correspondence as possible with the *PPC-TTC* model, KaiC is

produced in its fully phosphorylated, but active, state, C_6. Because the flip rate from C_6 to $\tilde{C}_6$ is much faster than the dephosphorylation rate, however, this has essentially no effect on the dynamics. In contrast, the reaction from $\tilde{C}_0 \to C_0$ is critical: Omitting it would yield a model that behaves *exactly* as the TTC-only model—dephosphorylation would merely change the phosphorylation *label* of KaiC, but not the dynamics of *kaiC* repression. In order for protein modification to have an effect on the temporal regulation of *kaiC* repression, it is essential that KaiC can leave the modification states in which it represses *kaiC* via a reaction other than degradation. It should also be noted that, in order to compare the *PMS-TTC* model with the *PPC-TTC* model, the dephosphorylation reactions have the same rates as in the *PPC-TTC* model. As for the *TTC-only* model, when μ is varied, both the protein synthesis rate β_c and the delay in protein synthesis τ are adjusted so that the average KaiC concentration and the oscillation period remain constant. When $\mu \ll k_{dps}$, the gene-repressing phosphoforms turn into the nonrepressing C_0 state via protein dephosphorylation before they are degraded, and one might thus think that the model's behavior is completely independent of μ in this limit. However, C_0 is part of the total KaiC concentration, which we fix by adjusting β_c for each μ; and because β_c does affect the behavior of the system as described below, μ remains an important control variable, even when $\mu \ll k_{dps}$. The magenta line of Fig. S2*E* shows the correlation number of cycles $n_{1/2}$ as a function of the protein degradation rate μ for $V = 1\ \mu m^3$ for the *PPC-TTC* model. It is more robust than the *TTC-only* model, with sustained oscillations for lower values of the protein degradation rate. Nonetheless, the oscillations still cease to exist for small enough μ.

Minimal UPPC-TTC model. This model probes the ability of the TTC to synchronize the PPC. To this end, it combines a TTC with an unsynchronized protein phosphorylation cycle (UPPC). Each protein undergoes a full cycle of protein modification steps as in the original PPC, but the cycles of the individual proteins (KaiC hexamers) are not synchronized as in the original PPC —KaiA, and thus the differential-affinity synchronization mechanism, has been removed. The model is defined by the reactions

$$C_6 \xrightarrow{f_6} \tilde{C}_6, \qquad \tilde{C}_0 \xrightarrow{b_0} C_0, \qquad C_i \xrightarrow{k_{pf}} C_{i+1}, \qquad \text{[S27]}$$

$$C_i \underset{k_{dps}}{\overset{k_{ps}}{\rightleftarrows}} C_{i+1}, \qquad \tilde{C}_i \underset{\tilde{k}_{dps}}{\overset{\tilde{k}_{ps}}{\rightleftarrows}} \tilde{C}_{i+1}, \qquad \text{[S28]}$$

$$\varnothing \xrightarrow[\tau;\sigma_\tau]{\beta_c K^4/(K^4+[R]^4)} C_6, \qquad C_i, \tilde{C}_i \xrightarrow{\mu} \varnothing. \qquad \text{[S29]}$$

Here, $[R] = \sum_{i=0}^{6} [\tilde{C}_i]$ is, as in the other minimal models, the total concentration of the KaiC phosphoforms that repress *kaiC* expression. The light blue line of Fig. S2*E* shows the robustness of this model, $n_{1/2}$, as a function of the protein turnover rate μ for $V = 1\ \mu m^3$; when μ is varied, the protein synthesis rates are adjusted to keep the average protein concentrations constant. (As with the *PPC-TTC* model, the period is largely determined by the phosphorylation cycle.) Its behavior in the limit of high protein degradation rate is similar to that of the *PMS-TTC* model, but the oscillations disappear more gradually as μ is decreased, and even in the limit of low protein turnover rate, the system shows damped oscillations, leading to a $n_{1/2}$ value of about 1–2 days.

Toward a mechanism for robustness. In section E of the main text, we argued that the *PPC-TTC* model is easily understood in the limits of low and high degradation rates: At low degradation rates, a TTC by itself must fail, because it can generate only large amplitude oscillations if proteins are synthesized and destroyed on times scales faster than the oscillation period; one thus expects that the *PPC-TTC* clock is driven primarily by the PPC for small μ. On the other hand, at high degradation rates, most KaiC proteins are destroyed before they can complete a full phosphorylation cycle, reducing the importance of the PPC. The TTC should thus be dominant when μ is large. These expectations are borne out by the simulation results of Fig. S3. For small μ (Fig. S3*A*), the total KaiC concentration is nearly constant in time, and oscillations in the concentration of KaiC phosphoforms that repress *kaiC* expression ([R]) are driven almost entirely by the protein modification cycle of the PPC. For large μ (Fig. S3*B*), in contrast, [R] tracks the total KaiC concentration almost perfectly, indicating that the oscillations arise primarily from periodic protein synthesis and degradation.

Although these limiting cases go a long way toward unraveling the behavior of the *PPC-TTC* model, they do not entirely explain the crossover regime when $1/\mu$ is of order of the clock period and the combined *PPC-TTC* performs far better than the TTC or PPC alone. The *PMS-TTC* and *UPPC-TTC* models allow us to move away from the limiting cases and to examine how a PPC can *enhance* a TTC, and vice versa, in this crossover regime.

To explain why a PMS can enhance the stability of a TTC, we show in Fig. S3*C* time traces of the concentrations of the individual KaiC phosphoforms that repress *kaiC* in the *PMS-TTC* model, as well as their sum [R]; for comparison, we also show a time trace of the KaiC concentration [C] in the *TTC-only* model. In the *TTC-only* model, the concentration of KaiC varies slowly and unreliably. In contrast, in the *TTC-PMS* model, the total repressor concentration [R] switches rapidly and strongly between a value that is well below the repression threshold and one that is well above it; this occurs because the concentrations of the individual KaiC phosphoforms rise and fall sharply as a result of the sequence of protein modification steps. These strong oscillations are beneficial because they minimize the effect of fluctuations in the repressor concentration on the timing of gene repression. To demonstrate this more clearly, we analytically compute for the *TTC-only* and the *PMS-TTC* models the distribution of times it takes to cross the gene repression threshold $[R] = K$, assuming that initially N molecules are present in the system that then decay either via protein degradation only, as in the *TTC-only* model, or via a combination of protein degradation and protein modification, as in the *PMS-TTC* model (see *Appendix* for details).

Fig. S3*D* shows the distribution of crossing times for both the *TTC-only* model and the *PMS-TTC* model, and for different values of the protein degradation rate μ. It is seen that the crossing-time distribution of the *PMS-TTC* model is narrower than that of the *TTC-only* model, especially when the protein degradation rate is lower than the protein modification rate. Although in the *TTC-only* model gene repression is relieved only via protein degradation, involving a single Poisson process, in the *PMS-TTC* model gene repression can also be relieved via protein modification, which involves a sequence of Poissonian steps. The sequence of Poissonian steps leads to a narrower waiting-time distribution for crossing the repression threshold, and this explains why a protein modification sequence, which is a key characteristic of the PPC, can enhance the robustness of a TTC.

Although the protein modification sequence makes the *PMS-TTC* model more robust than the *TTC-only* model (Fig. S2*E*), the *PMS-TTC* model nonetheless is subject to the same fundamental bounds on its amplitude as a function of μ, and it therefore does fail for protein degradation rates lower than about $0.05\ h^{-1}$. If we examine the simulation results in this regime in more detail, we can see that the immediate cause of the failure is an accumulation of molecules in the C_0 state, leading the concentrations of KaiC phosphoforms that repress gene expression to drop below the re-

pression threshold permanently. The *UPPC-TTC* model differs from the *PMS-TTC* model in that it does not permit proteins to accumulate in one state, but instead includes an entire *cycle* through which molecules can be recycled to the $\tilde{C}_6$ state. With such a cycle, coherent oscillations are in principle possible down to $\mu = 0$; all that is required is a mechanism to synchronize the cycles of the different KaiC hexamers. In the models in which only a PPC is present, this synchronization is of course accomplished by the differential-affinity mechanism, but a moment's reflection reveals that the TTC must also have a synchronizing effect: When, once each oscillation period, a burst of proteins is produced in the C_6 state, the distribution of phosphoforms not only shifts toward C_6, it also becomes narrower. Or, to phrase the argument slightly differently, while all KaiC hexamers are removed from the system at a rate that does not depend on the modification state, meaning that the protein removal process has no effect on the breadth of the phosphoform distribution, they are replaced by a synchronized group of proteins all in the same phosphorylation state, which means that the synthesis process does tend to narrow the distribution. This necessarily acts to synchronize the oscillation as a whole. With the *UPPC-TTC* model, in which this is the only synchronizing influence present, we can examine quantitatively how strong this effect is. To this end, we need to examine the stability of the *UPPC-TTC* in the regime $0.02 < \mu < 0.05$ h^{-1}. In this regime, the *UPPC-TTC* model is much more stable than the *TTC-only* and the *PMS-TTC* models, showing that the PPC is the principal driver in this regime. Moreover, the stability of the *UPPC-TTC* model in this regime is higher than that in the limiting regime of low growth rate. This difference is due to the synchronizing effect of the TTC on the PPC. This idea is supported by the fact that the $n_{1/2}$ values for the *UPPC-TTC* model and the *PPC-TTC* model begin to increase at almost the same degradation rate μ. Taken together, these observations strongly suggest that the increased robustness of the *PPC-TTC* model in the crossover regime can be attributed in large measure to the additional synchronizing effect of the TTC.

In summary, our analysis suggests that at low protein turnover rates, where $n_{1/2}^{PPC\text{-}TTC} \approx n_{1/2}^{PPC} \gg n_{1/2}^{TTC}$, the PPC is the principal driver of the circadian clock; at somewhat higher μ, where $n_{1/2}^{PPC\text{-}TTC} > n_{1/2}^{PPC} \gg n_{1/2}^{TTC}$, the PPC still drives the clock, but it needs help from the TTC to create macroscopic oscillations out of the phosphorylation cycles of the individual hexamers; at even higher values of μ, where $n_{1/2}^{PPC\text{-}TTC} > n_{1/2}^{TTC} \gg n_{1/2}^{PPC}$, the TTC is the principal pacemaker, but its stability is enhanced by the protein modification sequence of the PPC; and at the highest turnover rates, where $n_{1/2}^{PPC\text{-}TTC} \approx n_{1/2}^{TTC} \gg n_{1/2}^{PPC}$ the TTC is the sole driver of the clock.

S3. *PPC-TTC* Model: Rhythms of *kaiBC* Expression when *kaiA* Is Overexpressed. Kitayama et al. have shown that *kaiBC* expression oscillates with a circadian period in the presence of an excess of KaiA, although it is not clear whether these oscillations are sustained or damped (17). Our *PPC-TTC* model of the main text, which is described by **S1**–**S5** and **S12**–**S14** above, generates oscillations in *kaiBC* expression with a period of 24 h when *kaiA* is overexpressed threefold, as shown in Fig. S4*A*. This figure shows that the phosphorylation level also exhibits weak oscillations, which are not seen experimentally; this is due to the fact that our PPC model neglects phosphorylation of inactive KaiC, which is known to occur at high KaiA concentrations (8). To rectify this, we have extended our model to include KaiA-stimulated phosphorylation of inactive KaiC, using the same reactions as those used for active KaiC; specifically, we add to the reactions of **S1**–**S5** and **S12**–**S14** the following reactions:

$$A_y B_x \tilde{C}_i + A \underset{\tilde{k}_i^{Ab}}{\overset{\tilde{k}_i^{Af}}{\rightleftarrows}} A_y B_x \tilde{C}_i A \xrightarrow{\tilde{k}_{pf}} A_y B_x \tilde{C}_{i+1} + A, \qquad \textbf{[S30]}$$

for each phosphorylation level i; the rate constants equal those of the corresponding reactions of active KaiC, except that the KaiA-KaiC association rate is reduced by a factor of 100. All other rate constants are as in Table S1. We also include autoactivation of RpaA via

$$\tilde{R} \xrightarrow{k_a^m} R, \qquad \textbf{[S31]}$$

with $k_a^m = 25$ h^{-1}. Autoactivation of RpaA becomes necessary because the concentrations of the KaiC phosphoforms that activate RpaA become very low when KaiA is in excess. (The freshly injected KaiC hexamers do not make it to the bottom of the phosphorylation cycle because of the excess KaiA.) This model not only matches the in vitro observation that when an excess of KaiA is added during the dephosphorylation phase, the phosphorylation level of KaiC rises immediately (8), but also reproduces the in vivo oscillations of the total amount of KaiC when KaiA is overexpressed (17), as shown in Fig. S4*B*.

S4. Robustness of the *PPC-TTC* Model to Parameter Variations. In this section, we discuss how robust our *PPC-TTC* model is to variations in a number of parameters. In the next subsection we show that the results are insensitive to details of the pathway that couples the PPC with the TTC. In subsection S4.2 we show that bursts in gene expression hardly reduce the stability of the clock. In the next two subsections we show that the stability of the clock is highly insensitive to the value of the Hill coefficient of gene repression as long as it is larger than one, and quite insensitive to the variance in the delay of protein synthesis. In essence, combining a PPC with a TTC enhances the robustness of the clock to variations in the parameters of the TTC, such as the magnitude of bursts in gene expression, the Hill coefficient, and the width of the delay distribution. Finally, in subsection S4.5 we study a model in which cell growth, cell division, and binomial partitioning of proteins upon cell division are modeled explicitly and show that, due to the stabilizing effect of the PPC, its behavior is similar to the model of the main text. In the next section, section S5, we discuss a different *PPC-TTC* model, namely one that is based upon the model of the PPC developed by Rust et al. (8).

S4.1. Results are independent of details of the output pathway. In this section, we show that the precise choice of the KaiC phosphoforms that activate and repress RpaA is not critically important for the existence of oscillations. Table S2 shows the different models that we have considered, and Fig. S5 *A*–*C* shows their time traces. It is seen that the time traces are very similar to those of the *PPC-TTC* model of the main text, which is model a in Table S2. The most significant difference can be observed for the time trace of RpaA in models d and e. In these models, not only C_xA activates RpaA, but also C_x, thus KaiC that is not bound to KaiA. The concentration of C_xA reaches zero during the dephosphorylation phase, and, as a result, the concentration of RpaA becomes zero during this phase in models a–c. However, the concentration of C_x does not reach zero during the dephosphorylation phase, and consequently, there is some residual activation of RpaA during this phase in models d and e. Nevertheless, RpaA activation during the dephosphorylation phase in these models does not manifest itself in the time traces of KaiC, because the concentration of active RpaA is still below the threshold for *kaiBC* expression. The oscillations of the phosphorylation level and total KaiC concentration are thus fairly similar in all models, although models d and e are less robust.

S4.2. The effect of bursts. In the *PPC-TTC* model of the main text, described in section S1 of this *SI Text*, we have concatenated transcription and translation into one gene-expression step. Moreover, we have ignored promoter-state fluctuations. Allowing

for the explicit formation and translation of mRNA (11), as well as for slow promoter-state fluctuations (12, 13), could lead to bursts in protein synthesis, which are expected to lower the robustness of the TTC. This could potentially lower the stability of the clock. To address this, we have performed simulations of a model in which KaiB and KaiC are produced in bursts. We assume that 5 KaiC hexamers and 15 KaiB dimers are formed in each gene-expression reaction (rather than the 1 and 3 of **S13**); this corresponds to typical burst sizes observed experimentally (11) in *Escherichia coli*. Formula **S13** is thus replaced by

$$\varnothing \xrightarrow[\tau\pm\sigma_\tau]{\beta_c[\mathrm{R}]^4/(\mathrm{K}^4+[\mathrm{R}]^4)} 5\mathrm{C}_6 + 15\mathrm{B}. \qquad \textbf{[S32]}$$

Fig. S5*D* shows the resulting phase diagram. It is similar to Fig. 4 of the main text, which shows the results of the *PPC-TTC* model without bursts in gene expression. The robustness of the model with bursts is lower, but not very much so: $n_{1/2} = 150$ for the model with bursts versus $n_{1/2} = 195$ for the model without bursts shown in the main text ($\mu = 0.03\ \mathrm{h}^{-1}$ and $V = 1\ \mu\mathrm{m}^3$ in both cases). We believe that this relatively small reduction in the clock's stability is due to the stabilizing effect of the PPC.

S4.3. Robustness to varying the Hill coefficient. Fig. S5*E* shows for the full *PPC-TTC* model the correlation number of cycles, $n_{1/2}$, as a function of the degradation rate μ for $V = 1\ \mu\mathrm{m}^3$, for four different values of the Hill coefficient of gene repression (see **7** of the main text and **S13**). It is seen that the stability of the clock is highly insensitive to the value of the Hill coefficient, except when the degradation rate is high: For $\mu > 0.1\ \mathrm{h}^{-1}$, the oscillator becomes unstable when the Hill coefficient drops from 2 to 1. For lower values of μ the PPC plays an important role in driving and stabilizing the clock; in fact, for $\mu < 0.02\ \mathrm{h}^{-1}$ the PPC is the sole driver, which means that in this regime the clock is not sensitive at all to variations in the parameters of the TTC (as long as the average concentrations and copy numbers remain constant). For $\mu > 0.1\ \mathrm{h}^{-1}$, however, the TTC becomes the principal driver of the clock, which means that now the system does become sensitive to variations in the parameters of the TTC. It is known that oscillators built on only negative transcriptional feedback require a Hill coefficient that is larger than one to become stable (14). Our results are in line with these observations.

S4.4. Robustness to the variance in the delay of protein synthesis. Fig. S5*F* shows for the full *PPC-TTC* model the correlation number of cycles $n_{1/2}$ as a function of the degradation rate μ and the width of the distribution of the delay in protein synthesis, σ_τ (see **S13**). It is seen that because of the stabilizing effect of the PPC the clock is essentially insensitive to variations in σ_τ. Only for $\mu > 0.1\ \mathrm{h}^{-1}$, when the TTC becomes the principal pacemaker of the clock, does $n_{1/2}$ decrease when σ_τ becomes larger than 3 h.

S4.5. PPC-TTC model with volume growth and binomial partitioning. Living cells constantly grow and divide, and proteins thus have to be synthesized to balance dilution. In the main text, we argued that the principal effect of dilution is to introduce an effective degradation rate set by the cell doubling time. Here, we show that this is indeed the case: We study a model in which growth, cell division, and binomial partitioning of the proteins upon cell division are modeled explicitly (15) and show that its qualitative behavior is similar to the model of the main text, in which the volume is held constant and protein degradation occurs at a rate that is constant in time.

The model we consider here is the *PPC-TTC* model presented in the main text, but with the degradation reaction, **9**, replaced by a scheme in which the bacterial volume V grows exponentially as

$$V(t) = V_0 e^{t\frac{\ln 2}{T_\mathrm{d}}}, \qquad \textbf{[S33]}$$

where T_d denotes the doubling time after which the volume reaches twice its minimum V_0 and cell division is triggered. Division includes dividing the volume by two, partitioning the proteins binomially (15), and deleting events on the queue of the delay associated with the KaiC production reaction with a probability of 0.5 for each daughter cell. To compare the results of this model with those from the main text, we take $T_\mathrm{d} = \ln 2/\mu$, where μ is the protein degradation rate of the model in the main text; if proteins were to decay only by dilution in a cell with a doubling time T_d, then μ would be the effective protein degradation rate; if proteins are also degraded actively, then $\mu = \ln 2/T_\mathrm{d}$ is a lower bound on the actual degradation rate.

Fig. S5 *G* and *H* show time traces of the total KaiC concentration and the KaiC phosphorylation level for this refined model. It is seen that the oscillations of the total KaiC concentration are more noisy than those in the model in which the Kai proteins are degraded with rates that are constant in time (Fig. S1*C*). Clearly, binomial partitioning is a major source of noise, with the random removal of items from the queue associated with the KaiC synthesis reaction being the largest source of noise. Nonetheless, the oscillations of the KaiC phosphorylation level are much less affected, with the correlation number of cycles being $n_{1/2} = 88$. Indeed, while this model combining a TTC with a PPC is fairly robust, an oscillator with exponential volume growth and binomial partitioning built upon a TTC alone, is not stable. This supports our statement in the main text that a PPC can strongly enhance the robustness of a TTC. In future work, we will systematically study the effect of bursts in gene expression and binomial partitioning.

S5. An Alternative *PPC-in Vitro* Model: The Rust Model. In the main text, we argue that the synergy between a transcription–translation cycle and a protein modification cycle is a generic feature of clocks that exploit both cycles. To support this claim, we have studied a model in which our model of the PPC is replaced by that of Rust et al. (8). This model describes a phosphorylation cycle at the level of KaiC monomers, rather than KaiC hexamers as in our model. In the Rust model, each KaiC monomer cycles between an unphosphorylated state "U," a singly phosphorylated state "T," where KaiC is phosphorylated at threonine 432, a doubly phosphorylated state "ST," where KaiC is phosphorylated at threonine 432 and serine 431, and a singly phosphorylated state "S," where KaiC is phosphorylated at serine 431 (8, 16). This cycle is described by the reactions

$$\mathrm{U} \leftrightarrow \mathrm{T}, \qquad \mathrm{T} \leftrightarrow \mathrm{ST}, \qquad \mathrm{ST} \leftrightarrow \mathrm{S}, \qquad \mathrm{S} \leftrightarrow \mathrm{U} \qquad \textbf{[S34]}$$

with reaction rates given by equation 5 of the supplementary material of Rust et al. (8). These rates depend on the concentration of free KaiA, which is sequestered by KaiC in the S state. We model KaiA sequestration explicitly:

$$\mathrm{S} + \mathrm{A} \leftrightarrow \mathrm{AS}, \qquad \mathrm{AS} + \mathrm{A} \leftrightarrow \mathrm{A_2S}. \qquad \textbf{[S35]}$$

We picture sequestration to be fast and we picked a forward rate of $1.72 \cdot 10^{12}\ 1/\mathrm{Mh}$ and a backward rate of h^{-1} for both equations above. Dephosphorylation of KaiC in the S state might occur even when KaiA is bound, in which case the KaiA protein is released from the complex. We define the output signal as

$$p(t) = \frac{[\mathrm{T}] + [\mathrm{ST}] + [\mathrm{S}] + [\mathrm{AS}] + [\mathrm{A_2S}]}{[\mathrm{U}] + [\mathrm{T}] + [\mathrm{ST}] + [\mathrm{S}] + [\mathrm{AS}] + [\mathrm{A_2S}]}, \qquad \textbf{[S36]}$$

which resembles the phosphorylation ratio in the case where we cannot distinguish between singly and doubly phosphorylated

KaiC. The denominator in the above expression is also the total KaiC monomer concentration. We use the same concentrations as Rust et al., [KaiA] = 1.3 μM (active KaiA monomers) and [KaiC] = 3.4 μM (KaiC monomers), and simulate this model using the Gillespie algorithm (2).

When we simulate this model for a volume $V = 1\ \mu m^3$, we find a period of $L = 21.4$ h and a decay constant for the autocorrelation function of $\tau_d = 128$ h. The corresponding correlation number of cycles is $n_{1/2} = 30$, which is lower than that observed experimentally, $n_{1/2} = 166 \pm 100$ (5), and lower than that of the PPC developed by us (1), for which $n_{1/2} \approx 200$ (see Fig. 2 of the main text). This is because the model of Rust et al. features a phosphorylation cycle at the level of KaiC monomers rather than KaiC hexamers as in our model. The concomitant reduction in the total number of phosphorylation steps in the cycle reduces the robustness in the model of Rust et al. (8).

S5.1. An alternative PPC-in vivo model: The Rust model with constant protein synthesis and degradation. To study the behavior of the model of Rust et al. (8) under conditions in which cells grow and divide, we have to include protein degradation and make up for this by protein synthesis. As in the main text, when we vary the protein degradation rates, we adjust the protein synthesis rates such that the average protein concentrations are unchanged and similar to those used in the in vitro experiments (3, 4).

Fig. S6*A* shows the results for this model. They are qualitatively the same as those of Fig. 3 of the main text: The robustness decreases with decreasing volume and increasing degradation rate. Hence, not only in our model but also in that of Rust et al. (8), protein degradation can cause the oscillations to disappear. This supports our claim that a protein modification oscillator cannot function on its own when the cell's growth rate is high enough.

S5.2. An alternative PPC-TTC model: The Rust model with a TTC. We will now show that a TTC can resurrect the PPC of Rust et al. (8). We model the TTC as

$$\varnothing \underset{\tau,\sigma_\tau}{\overset{\beta_c[\mathrm{R}]^4/(\mathrm{K}^4+[\mathrm{R}]^4)}{\longrightarrow}} \mathrm{ST}, \qquad \varnothing \overset{\beta_a}{\rightarrow} \mathrm{A}, \qquad \varnothing \overset{\beta_r}{\rightarrow} \tilde{\mathrm{R}}, \qquad \textbf{[S37]}$$

$$\tilde{\mathrm{R}} + \mathrm{T} \overset{k_a}{\rightarrow} \mathrm{R} + \mathrm{T}, \qquad \mathrm{R} + \mathrm{A}_x\mathrm{S} \overset{k_i}{\rightarrow} \tilde{\mathrm{R}} + \mathrm{A}_x\mathrm{S}, \qquad x \in \{0,1,2\}, \qquad \textbf{[S38]}$$

$$\mathrm{A},\mathrm{R},\tilde{\mathrm{R}},\mathrm{U},\mathrm{S},\mathrm{A}_x\mathrm{S},\mathrm{T},\mathrm{ST} \overset{\mu}{\rightarrow} \varnothing, \qquad \textbf{[S39]}$$

where the first line describes the production of proteins to counteract their degradation and the second line summarizes the RpaA signaling pathway, where KaiC that is phosphorylated at the T site activates RpaA and KaiC that is phosphorylated at the S site represses RpaA activation. The parameters in this model are $\beta_c = 1.16$ μM/h, $\mathrm{K} = 0.058$ μM, $\beta_a = 0.13$ μM/h, $\beta_r = 0.058$ μM/h, $k_a = k_i = 1.71 \cdot 10^9$ 1/Mh, $\mu = 0.1\ \mathrm{h}^{-1}$, and the delay is $\tau = (3 \pm 0.3)$ h. Fig. S6*B* shows the results of this model at a volume $V = 1\ \mu m^3$. Analyzing the autocorrelation function, we find a period $L = 22.5$ h and a correlation decay time of $\tau = 1{,}832$ h leading to a correlation number of cycles of $n_{1/2} = 402$. Clearly, a TTC can also resurrect the PPC of Rust et al. (8), supporting our claim that the qualitative results of the main text should apply to any biological system that exploits both a protein modification cycle and a protein synthesis cycle to generate circadian rhythms.

S6. *PPC-TTC* Model: Period as a Function of Cell Volume and Protein Degradation Rate. Fig. S7 shows the period of the oscillation of the KaiC phosphorylation level in the full *PPC-TTC* model of the main text (**1**–**9**) as a function of the cell volume and the protein degradation rate. As before, the protein synthesis rates are adjusted such that the average protein concentrations are constant and similar to those used in the in vitro experiments (3, 4). It is seen that the dependence of the oscillation period on the cell volume and protein degradation rate is rather weak. This is because the rhythm of the clock is dictated by the PPC, which is insensitive to the absolute rates of protein synthesis and decay. We note here that the period of the oscillation, as well as its amplitude, would change if the *ratio* of the concentrations of the Kai proteins were changed. Although the dependence of both the amplitude and the period of the in vitro PPC on the ratio of the concentrations of the Kai proteins has been characterized in detail (3, 4), the dependence of the in vivo oscillator on their ratio has not been studied experimentally.

S7. Measuring the Robustness. In this section, we discuss how we calculate the correlation number of cycles $n_{1/2}$ for our various models. We begin with some theoretical background: Consider a phase variable $\varphi(t)$ that increases with an average frequency ω and is also subject to noise. Its time evolution can be written as

$$\frac{d\varphi(t)}{dt} = \omega + \xi(t) \quad \text{with } \langle \xi(t)\xi(t') \rangle = \sigma^2 \delta(t - t'). \qquad \textbf{[S40]}$$

Here $\xi(t)$ is Gaussian white noise of strength σ^2, and $\langle \circ \rangle$ indicates averaging over different realizations of the noise. Integrating the equation with the initial condition $\varphi(0) = 0$ yields

$$\varphi(t) = \omega t + \mathscr{W}(t), \qquad \textbf{[S41]}$$

where $\mathscr{W}(t)$ is a Gaussian random variable with mean zero and variance

$$\langle (\varphi(t) - \omega t)^2 \rangle = \sigma^2 t. \qquad \textbf{[S42]}$$

From this, we can construct an oscillating signal

$$x(t) = x_0 + a \cdot \sin \varphi(t) \qquad \textbf{[S43]}$$

with mean x_0 and amplitude a. The autocorrelation function of **44** is then

$$\mathrm{C}(t') = \frac{\langle \delta x(t) \delta x(t + t') \rangle}{\langle \delta x(t)^2 \rangle} = e^{-\frac{1}{4}\sigma^2 |t'|} \cdot \cos(\omega t'), \qquad \textbf{[S44]}$$

where $\delta x(t) \equiv x(t) - x_0$ is the deviation of the signal from its average value x_0. We thus expect that the correlation function is a sinusoid modulated by a single exponential decay.

S7.1. Incorporating amplitude noise. Because the phase is the only "soft" direction of the dynamical system, one generically expects any noisy oscillator at long times to act similarly to the simple model of a phase oscillator just described. Nonetheless, a more realistic description would also include a fluctuating amplitude. We incorporate this behavior phenomenologically by including a time dependence in the amplitude:

$$a \rightarrow a(t) = a_0 + \xi_{(a)}(t) \Rightarrow x(t) = x_0 + [a_0 + \xi_{(a)}(t)] \cdot \sin[\omega t + \mathscr{W}(t)], \qquad \textbf{[S45]}$$

where $\xi_{(a)}(t)$ denotes a Gaussian white noise process of strength σ_a^2 and therefore neglects correlations in the amplitude fluctuations. We can again calculate the correlation function analytically. By definition, we have $\mathrm{C}(0) = 1$ for $t = 0$, but because $a(t)$ now contains a white noise term, $\mathrm{C}(t)$ jumps discontinuously to a smaller value for any $t > 0$. One finds

$$C(t') = \frac{\langle \delta x(t)\delta x(t+t')\rangle}{\langle \delta x(t)^2\rangle} = \underbrace{\frac{a_0^2}{a_0^2+\sigma_a^2}}_{=\nu} e^{-\frac{1}{4}\sigma^2|t'|}\cdot\cos(\omega t'), \qquad t' > 0. \tag{S46}$$

Considering the more natural case of a finite correlation time in the amplitude noise, the picture will only change slightly: Instead of jumping from 1 to ν at $t' = 0$, the envelope will undergo a smooth transition involving two time scales: a short time scale of the order of the correlation time of the amplitude fluctuations and a much longer time scale associated with the phase diffusion. In practice, we found that including amplitude fluctuations did not significantly change our estimate for $n_{1/2}$.

S7.2. Computing the correlation number of cycles. To calculate the correlation number of cycles $n_{1/2}$, we begin by using our simulation results to estimate the correlation function $C(t)$. After an initial equilibration phase of 500 h, we do simulations for 50,000 h. From these, we extract $N = 500{,}000$ values x_i for the time trace $x(t)$ at equidistant points in time, which we can then use to calculate the correlation function at times separated by an interval $\Delta t = 0.1$ h:

$$x_i = x(t_0 + i\cdot\Delta t), \qquad C(i\cdot\Delta t) = \frac{1}{(N-i)\cdot\langle\delta x^2\rangle}\sum_{j=0}^{N-i}\delta x_j\delta x_{j+i}. \tag{S47}$$

Here $x(t)$ is either the phosphorylation level $p(t)$ or the total concentration of KaiC hexamers. $p(t)$ is used for all cases except for models where there is only a TTC and a phosphorylation level cannot be defined.

Once $C(t)$ has been computed, it can be fitted to the form **S46** to determine the free parameters ν, σ^2, and ω. In practice we perform the fit using `gnuplot`, which in turn implements a Marquardt–Levenberg algorithm.

Finally, it remains to translate the fitted parameter values into an estimate of $n_{1/2}$. Eguchi et al. define $n_{1/2}$ as the number of cycles after which the standard deviation of the phase is π (7). Thus, we have

$$\sqrt{\langle[\varphi(L\cdot n_{1/2}) - \omega t]^2\rangle} = \pi \Rightarrow n_{1/2} = \frac{\pi^2}{L\sigma^2}, \tag{S48}$$

where $L = 2\pi/\omega$ denotes the period and we have used Eq. **S42** to solve the left equation for $n_{1/2}$. The value of $n_{1/2}$ is then obtained by substituting the fitted values for σ^2 and ω. Using this method we can reliably measure $n_{1/2}$ from 1 to 1,000. The upper bound is given by the fact that we compute the correlation function $C(t)$ only up to $t = 3{,}000$ h and therefore correlation functions that decay on much longer time scales are difficult to detect.

Concerning the error bar on the computed $n_{1/2}$, it should be noted that there are two distinct sources of error: one due to statistical fluctuations, and one due to systematic errors, e.g., that the correlation function cannot be fitted to Eq. **S46**. To estimate the former, for certain parameter values we repeated the procedure described above 32 times, i.e., we performed 32 independent simulations and computed the mean and the standard deviation of the set of 32 independently estimated values for $n_{1/2}$. For $V = 1\ \mu m^3$ and $\mu = 0.025\ h^{-1}$, this gave $n_{1/2} = 168 \pm 31$ (mean $\pm$ SD) for the combined *PPC-TTC* model. To address the second type of error, we also computed $n_{1/2}$ using two different methods. One is the method of Eguchi et al., which is based on examining the times at which the oscillation reaches its maximum in each cycle and thus does not assume any particular form like Eq. **S43** for the oscillating signal (7). The other method involves computing the width of the dominant peak in the power spectrum of the time traces. The three methods gave similar error bars and values for $n_{1/2}$ that agree within the error bar. Although all methods gave the same result, we found the method based on the correlation function (Eq. **S46**) more robust for noisy oscillations at low cell volumes.

Appendix: Crossing-Time Distribution in *TTC-Only* and *PMS-TTC* Models. We imagine that at $t = 0$ we have N repressor molecules, which can only decay; they can either decay via degradation only, as in the *TTC-only* model, or decay via a combination of degradation and a sequence of modification steps, as in the *PMS-TTC* model. The aim is now to compute the distribution of times the system crosses the repression threshold at a later time t. We imagine that the repression threshold is crossed when the number of molecules $M(t)$ at time t drops below M_c, thus when M goes from M_c to $M_c - 1$. This yields the following expression for the (normalized) distribution of crossing times:

$$P_c(t) = M_c q(t)\frac{N!}{(N-M_c)!M_c!}S(t)^{M_c-1}(1-S(t))^{N-M_c}, \tag{S49}$$

where $S(t)$ is the survival probability, which is the probability that a molecule has not decayed at later time t, and $q(t) = -\partial S(t)/\partial t$ is the probability per unit amount of time that a molecule, given that it is active at $t = 0$, decays at a later time t.

The task is now to compute $S(t)$. In the *TTC-only* model the molecules can decay only via degradation, and the survival probability is simply $S(t) = e^{-\mu t}$, where μ is the degradation rate. For the *PMS-TTC* model, we assume that the molecules start in the repressing $\tilde{C}_6$ state. They can then go through a sequence of irreversible protein modification steps $\tilde{C}_6 \to \tilde{C}_5 \to \cdots \to \tilde{C}_1 \to \tilde{C}_0$, and then switch to the nonrepressing C_0 state; moreover, in each state they can also decay via degradation. Each modification reaction occurs at a rate $\lambda = k_{dps}$, degradation proceeds with a rate μ, and the switch from $\tilde{C}_0$ to C_0 occurs with rate b_0. A molecule is still active as a repressor when it is in one of the $\tilde{C}_6,\tilde{C}_5,\cdots,\tilde{C}_1,\tilde{C}_0$ states, meaning that the survival probability is given by

$$S(t) = \sum_{i=0}^{6} P_i(t), \tag{S50}$$

where $P_i(t)$ is the probability that a molecule is in state $\tilde{C}_i$ at time t. For $i = 1,2,\ldots,5,6$, it is given by

$$P_i(t) = \frac{(\lambda t)^{6-i}}{(6-i)!}e^{-(\lambda+\mu)t}. \tag{S51}$$

Indeed, this equation holds for all the repressing states except the last one, because in this state $\tilde{C}_0$ the molecule can become nonrepressing not only via degradation, but also by switching to the nonrepressing state C_0 state. The probability of being in the $\tilde{C}_0$ at time t is

$$P_0(t) = \lambda\int_0^t dt' P_1(t')e^{-(b_0+\mu)t-t')}, \tag{S52}$$

$$= \frac{\lambda^6}{5!}e^{-(\mu+b_0)t}\int_0^t dt' t'^5 e^{-(\lambda-b_0)t'}, \tag{S53}$$

which can be solved analytically by iteratively integrating by parts. Clearly, if $b_0 = \lambda$ the above expression reduces to Eq. **S51** for $i = 0$. It is also clear that if $b_0 \to \infty$, $P_0(t)$ becomes zero and $S(t) = \sum_{i=1}^{6} P_i(t)$. Finally, if $\lambda = 0$, this model reduces to the *TTC-only* model.

1. van Zon JS, Lubensky DK, Altena PRH, ten Wolde PR (2007) An allosteric model of circadian KaiC phosphorylation. *Proc Natl Acad Sci USA* 104:7420–7425.
2. Gillespie DT (1977) Exact stochastic simulation of coupled chemical reactions. *J Phys Chem* 81:2340–2361.
3. Kageyama H, et al. (2006) Cyanobacterial circadian pacemaker: Kai protein complex dynamics in the KaiC phosphorylation cycle in vitro. *Mol Cell* 23:161–171.
4. Nakajima M, Ito H, Kondo T (2010) In vitro regulation of circadian phosphorylation rhythm of cyanobacterial clock protein KaiC by KaiA and KaiB. *FEBS Lett* 584 (5):898–902.
5. Mihalcescu I, Hsing W, Leibler S (2004) Resilient circadian oscillator revealed in individual cyanobacteria. *Nature* 430:81–85.
6. Kitayama Y, Iwasaki H, Nishiwaki T, Kondo T (2003) KaiB functions as an attenuator of KaiC phosphorylation in the cyanobacterial circadian clock system. *EMBO J* 22:2127–2134.
7. Eguchi K, Yoda M, Terada TP, Sasai M (2008) Mechanism of robust circadian oscillation of KaiC phosphorylation in vitro. *Biophys J* 95:1773–1784.
8. Rust MJ, Markson JS, Lane WS, Fisher DS, O'Shea EK (2007) Ordered phosphorylation governs oscillation of a three-protein circadian clock. *Science* 318:809–812.
9. Imai K, Nishiwaki T, Kondo T, Iwasaki H (2004) Circadian rhythms in the synthesis and degradation of a master clock protein KaiC in cyanobacteria. *J Biol Chem* 279:36534–36539.
10. Ermentrout B (2002) *Simulating, Analyzing, and Animating Dynamical Systems: A Guide to Xppaut for Researchers and Students* (SIAM, Philadelphia).
11. Ozbudak EM, Thattai M, Kurtser I, Grossman AD, van Oudenaarden A (2002) Regulation of noise in the expression of a single gene. *Nat Gen* 31:69–73.
12. Golding I, Paulsson J, Zawilski SM, Cox EC (2005) Real-time kinetics of gene activity in individual bacteria. *Cell* 123:1025–1030.
13. van Zon JS, Morelli M, Tănase-Nicola, Ten Wolde PR (2006) Diffusion of transcription factors can drastically enhance the noise in gene expression. *Biophys J* 91:4350–4367.
14. Gonze D, Halloy J, Gaspard P (2002) Biochemical clocks and molecular noise: Theoretical study of robustness factors. *J Chem Phys* 116:10997–11010.
15. Swain PS, Elowitz MB, Siggia ED (2002) Intrinsic and extrinsic contributions to stochasticity in gene expression. *Proc Natl Acad Sci USA* 99:12795–12800.
16. Nishiwaki T, et al. (2007) A sequential program of dual phosphorylation of KaiC as a basis for circadian rhythm in cyanobacteria. *EMBO J* 26:4029–4037.
17. Kitayama Y, Nishiwaki T, Terauchi K, Kondo T (2008) Dual KaiC-based oscillations constitute the circadian system of cyanobacteria. *Genes Dev* 22:1513–1521.

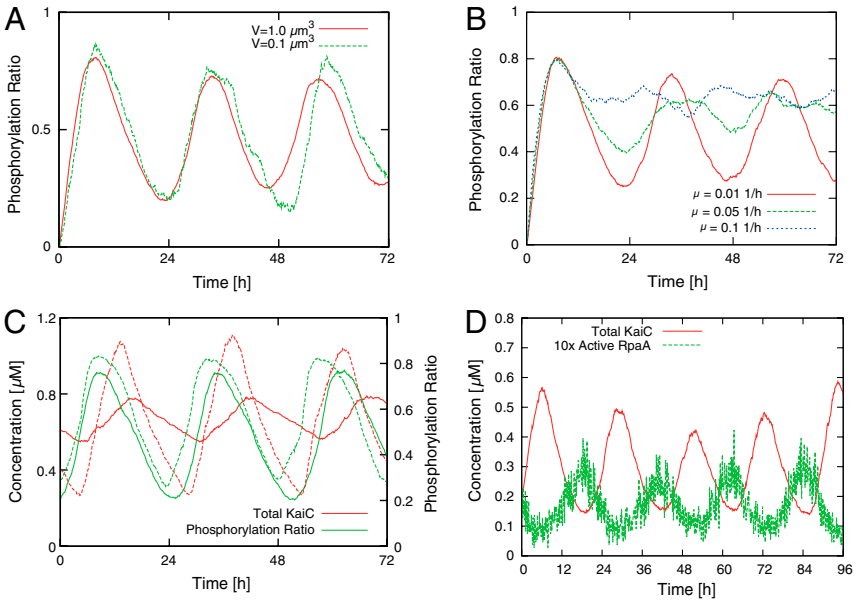

Fig. S1. Time traces of the different models studied in the main text. (*A*) *PPC-in vitro* model, a PPC model in which the concentration of each Kai protein is constant. Time traces of the phosphorylation level $p(t)$, defined as the fraction of monomers that is phosphorylated, for two different volumes. The correlation number of cycles, $n_{1/2}$, as a function of volume is shown in Fig. 2 of the main text. (*B*) *PPC-in vivo* model, a PPC model in which the Kai proteins are continually being produced and degraded. Time traces of the phosphorylation level $p(t)$ for three different degradation rates μ. The correlation number of cycles, $n_{1/2}$, as a function of volume and the degradation rate is shown in Fig. 3 of the main text. (*C*) *PPC-TTC* model, which combines a PPC with a TTC. Time traces of the phosphorylation level $p(t)$ and total KaiC concentration $[C]_T(t)$ for $V = 1$ μm^3 and $\mu = 0.03$ h^{-1} (solid lines) and $\mu = 0.1$ h^{-1} (dashed lines). The correlation number of cycles, $n_{1/2}$, as a function of volume and the degradation rate is shown in Fig. 4 of the main text. Time traces of RpaA are shown in Fig. S5*C*. (*D*) *TTC-only* model. Time traces of the concentrations of active RpaA and KaiC ($V = 1$ μm^3 and $\mu = 0.15$ h^{-1}). The (average) concentrations of KaiA, KaiB, and KaiC are those used in the in vitro experiments (3, 4): $[A]_T = 0.58$ μM; $[B]_T = 1.75$ μM; $[C]_T = 0.58$ μM. For other parameter values, see Table S1.

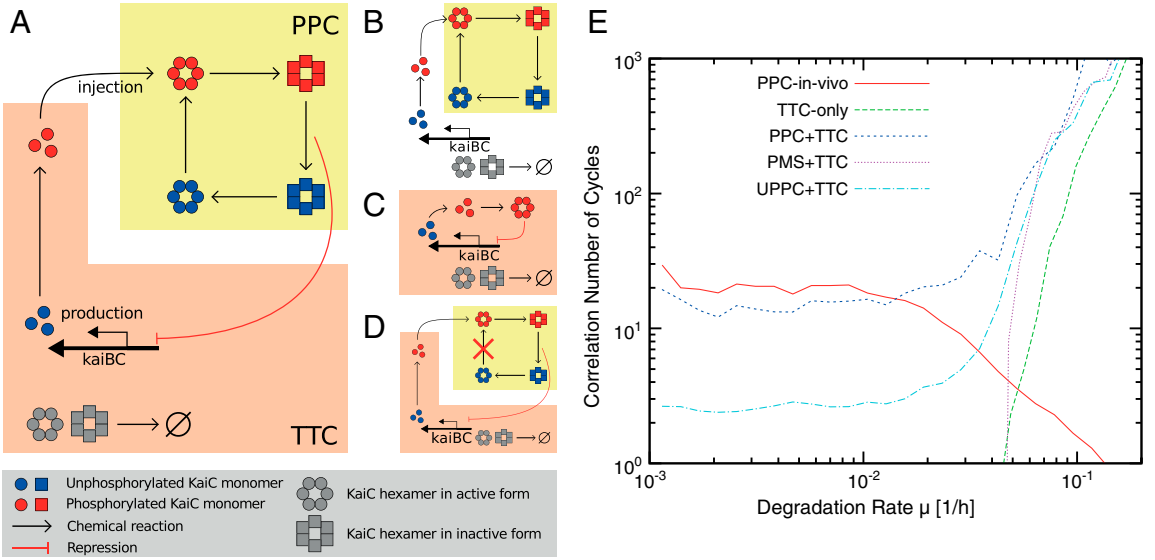

Fig. S2. Minimal models studied in section S2. (*A*–*D*) Cartoons; (*E*) robustness. (*A*) Minimal *PPC-TTC* model; (*B*) minimal *PPC-in vivo* model; (*C*) minimal *TTC-only* model; (*D*) minimal *PMS-TTC* model; this model exhibits a protein modification sequence; it is similar to the *PPC-TTC* model, except that the phosphorylation branch of the PPC is missing (as indicated by the red cross). In section S2 we also study the *UPPC-TTC* model, which is similar to the *PPC-TTC* model (*A*) except that the phosphorylation cycles of the individual KaiC hexamers are not synchronized via intermolecular interactions; KaiA, and thereby the synchronization mechanism of differential affinity, has been removed. (*E*) Correlation number of cycles, $n_{1/2}$, as a function of the protein degradation rate μ for $V = 1\ \mu m^{-3}$ for the different minimal models.

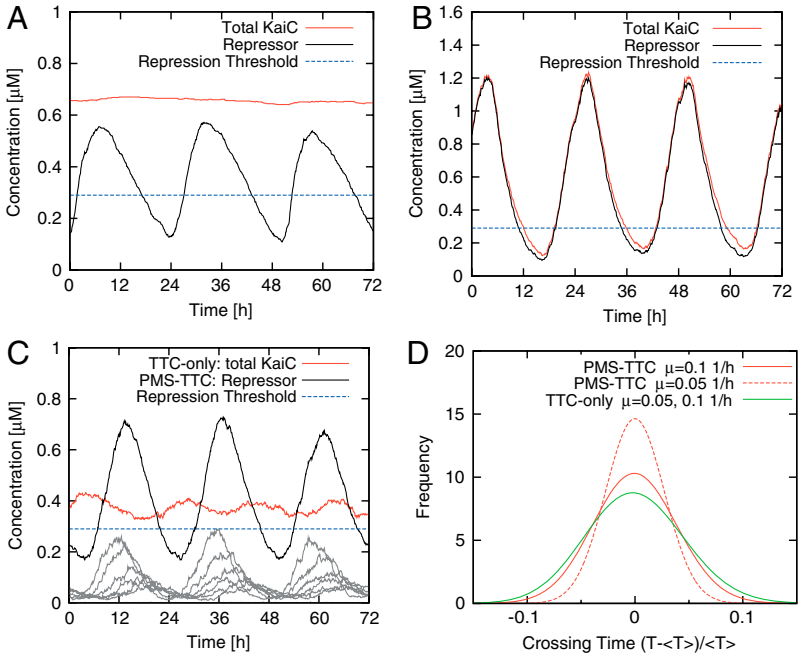

Fig. S3. The origin of the high robustness of the *PPC-TTC*. (*A* and *B*) Behavior of the *PPC-TTC* model in the limiting regimes of low and high protein degradation rates. Time traces of the total KaiC concentration (red line) and the sum of the concentrations of the KaiC phosphoforms that repress *kaiC* expression, $[\mathrm{R}](t) = \sum_{i=0}^{6}([\tilde{\mathrm{C}}]_i(t) + [\mathrm{A}\tilde{\mathrm{C}}_i] + [\mathrm{A}_2\tilde{\mathrm{C}}_i])$ (black line), for $\mu = 0.0017$ hr^{-1} (*A*) and $\mu = 0.2$ h^{-1} (*B*). The dotted blue line denotes the gene repression threshold. It is seen that for low protein degradation rates the oscillations in the concentrations of the various KaiC phosphoforms are dominated by the periodic protein modification of the PPC (the total KaiC concentration is essentially constant), whereas at high protein degradation rates they are driven by the periodic synthesis and decay of the TTC. (*C* and *D*) The importance of a protein modification sequence in the crossover regime of intermediate protein degradation rates. (*C*) Time traces of the total KaiC concentration, $[\mathrm{C}](t)$, in the minimal *TTC-only* model (red line), the total repressor concentration $[\mathrm{R}](t) = \sum_{i=0}^{6}[\tilde{\mathrm{C}}]_i(t)$ (black line), and the concentrations of the individual phosphoforms that repress *kaiC*, $[\tilde{\mathrm{C}}_i](t)$ (gray lines), in the *PMS-TTC* model, for $\mu = 0.09$ h^{-1} and $V = 1$ μm^3. The dashed blue line denotes the repression threshold. Note that while $[\mathrm{C}](t)$ of the *TTC-only* model exhibits only weak oscillations, the total repressor concentration $[\mathrm{R}](t)$ of the *PMS-TTC* model exhibits large amplitude oscillations due to the pronounced oscillations of the concentrations of the individual KaiC phosphoforms that repress *kaiC*, $[\tilde{\mathrm{C}}_i](t)$; the latter are the result of the protein modification sequence. (*D*) The distributions of times T (normalized by the average $\langle T \rangle$) the system crosses the repression threshold at $M_c = 500$ molecules, for different values of the degradation rate μ, given that at $t = 0$ $N = 1{,}000$ repressor molecules are put into the system. The repressors can either decay via first-order degradation only, as in the *TTC-only* model, or decay via a combination of degradation and a sequence of protein modification steps, as in the *PMS-TTC* model. The two distributions for the *TTC-only* model are identical, because protein decay is governed by a single Poisson step. The important point to note is that the distribution of the *PMS-TTC* model is significantly narrower than that of the *TTC-only* model, especially when μ is low. This is because of the sequence of Poissonian modification steps.

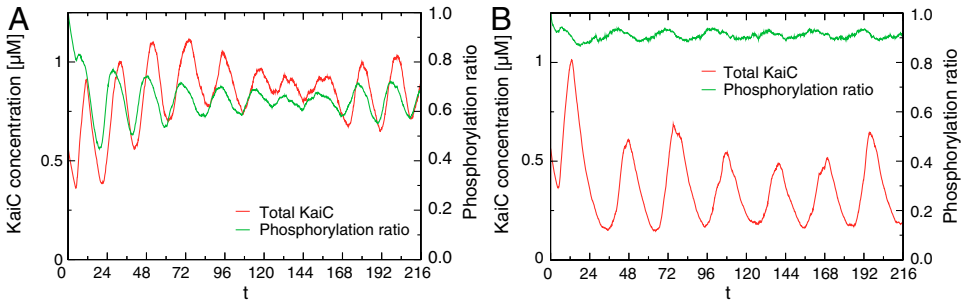

Fig. S4. The *PPC-TTC* model predicts oscillations in *kaiBC* expression when *kaiA* is overexpressed. (*A*) The original *PPC-TTC* model of **S1**–**S5** and **S12**–**S14**. (*B*) The modified *PPC-TTC* model, given by the original model of **S1**–**S5** and **S12**–**S14** but extended to include KaiA-stimulated phosphorylation of inactive KaiC (**S30**) and autoactivation of RpaA (**S31**). Note that the total amount of KaiC exhibits pronounced, albeit somewhat arrhythmic, oscillations, whereas the phosphorylation level is high and fairly constant. For both panels, the protein degradation rate is $\mu = 0.1$ h^{-1} and the volume is $V = 2.97$ μm^3; *kaiA* is overexpressed by a factor of 3.

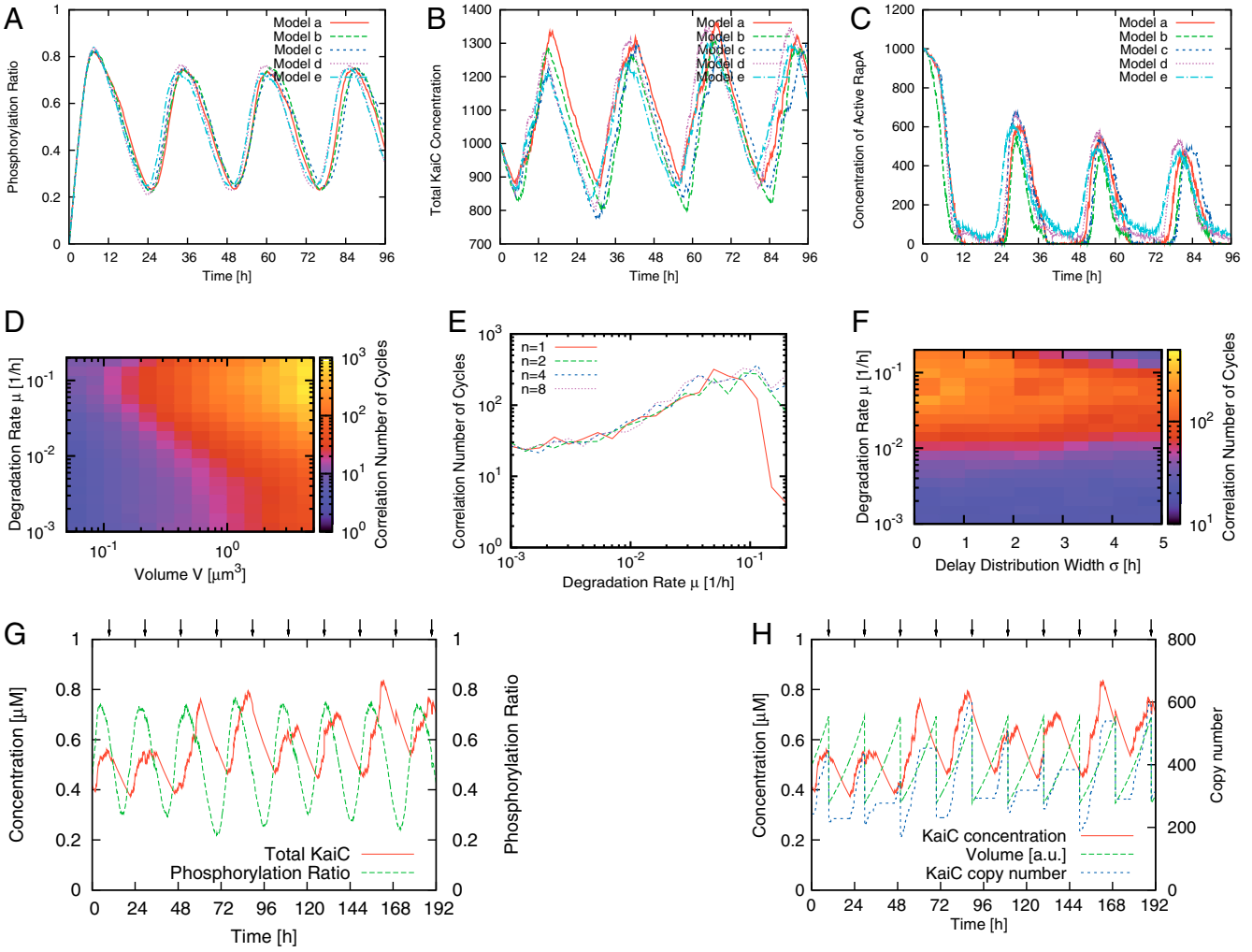

Fig. S5. Robustness of the *PPC-TTC* model to parameter variations. (*A*–*C*) Time traces of the stochastic simulations of models with different output pathways from the PPC to the TTC (see Table S2). The phosphorylation ratio (*A*), the total concentration of KaiC (*B*), and the concentration of RpaA (*C*) are fairly similar for all models studied. (*D*) The correlation number of cycles $n_{1/2}$ as a function of the degradation rate μ and the volume *V* for a *PPC-TTC* model that exhibits bursts in gene expression; upon a gene-expression event, 5 KaiC molecules are produced and 15 KaiB dimers. (*E*) $n_{1/2}$ as a function of μ for $V = 1\ \mu m^3$, for different values of the Hill coefficient *n* of gene repression (see Eq. **S13**). (*F*) $n_{1/2}$ as a function of μ and the width of the distribution of the delay in protein synthesis, σ_τ, for $V = 1\ \mu m^3$ (see **S13**). (*G* and *H*) Time traces of the *PPC-TTC* model modified to take into account cell division and binomial partitioning. Here, the cell divides when the volume reaches $V_m = 1.38\ \mu m^3$, which occurs every 20 h, as indicated by the arrows above the graph; a cell doubling time of 20 h corresponds to an effective degradation rate of $\mu = 0.035$ 1/h. The average volume is $V = 1\ \mu m^3$. (*G*) Time traces of the phosphorylation level and the total KaiC concentration. (*H*) Time traces of the total KaiC concentration, the KaiC copy number, and the volume. Note that the time trace of the total KaiC concentration is hardly affected when cell division happens to occur during the degradation phase, whereas it has a relatively large effect when cell division happens to occur during the KaiC production phase; this is because the removal of items from the queue associated with the KaiC synthesis reaction effectively lowers the synthesis rate; indeed this explains the change in slope in the KaiC concentration during the production phase.

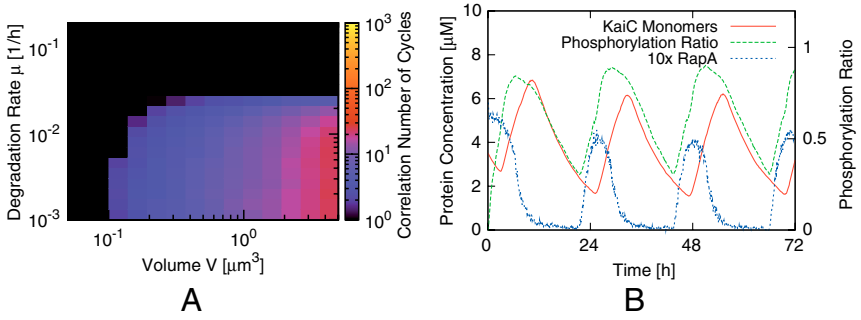

Fig. S6. Robustness of a *PPC-in vivo* (*A*) and a *PPC-TTC* model (*B*), where the PPC is based on the model of Rust et al. (8). (*A*) Contour plot of $n_{1/2}$ of the PPC model of Rust et al. but with production and degradation of Kai proteins with rates that are constant in time, as a function of the degradation rate μ and the volume *V*. (*B*) Time trace of the Rust model (8) extended to include a TTC for $V = 1$ μm^3. Both the total concentration of KaiC and the phosphorylation level of KaiC show stable oscillations. The messenger protein RpaA concentration is shown tenfold and crosses the threshold of K = 0.174 μM (≈100 molecules) reliably.

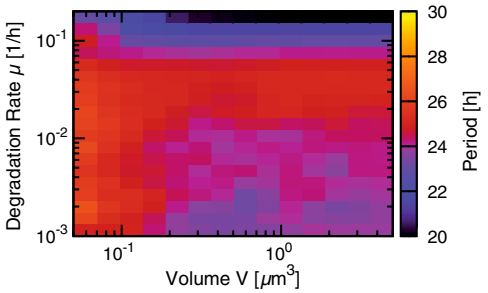

Fig. S7. Period of the oscillation in the KaiC phosphorylation level in the full *PPC-TTC* model of the main text as a function of cell volume and protein degradation rate. When the degradation rate is varied, the protein synthesis rates are adjusted such that the average protein concentrations are constant and similar to those used in the in vitro experiments (3, 4). The period is essentially independent of the volume and exhibits only a weak dependence on the degradation rate μ.

Table S1. The parameters used for the full models of the main text and the minimal models of section S2

Constant	Value	Constant	Value
PPC (**1–5** and **S1–S5**):			
k_{ps}, $\tilde{k}_{ps}$	0.025 1/h	k_{dps}, $\tilde{k}_{dps}$	100 1/h
k_{pf}	1.0 1/h		
f_i	$\{10^{-6},10^{-5},10^{-4},10^{-3},10^{-2},10^{-1},10\}$ 1/h	b_i	100 1/h
k_i^{Af}	$1.72 \cdot 10^{10}$ 1/M·h	k_i^{Ab}	$\{1,3,9,27,81,243,729\}$ 1/h
$\tilde{k}_i^{Bf}$	$1.72 \cdot 10^{9} \times \{0.001,0.1,1,1,1,1,1\}$ 1/M·h	$\tilde{k}_i^{Bb}$	$\{10,1,1,1,1,1,1\}$ 1/h
$\tilde{k}_i^{Af}$	$1.72 \cdot 10^{9} \times \{10^{-2},10^{3},10^{3},10^{3},10^{2},10^{-3},10^{-4}\}$ 1/M·h		
$\tilde{k}_i^{Ab}$	$\{10,1,1,1,1,1,10\}$ 1/h		
Deterministic PPC (Eqs. **S8–S11**):			
$\tilde{\kappa}_i^{Bf}$	$2.97 \cdot 10^{18} \times \{0.01,1,1,1,1,1,1\}$ 1/M²·h	$\tilde{\kappa}_i^{Bb}$	$100 \times \{10,1,1,1,1,1,1\}$ 1/h
K_i	$3.37 \cdot 10^{-25} \times \{\infty,100,1,1,100,\infty,\infty\}$ M²		
RpaA activation (**6** and **S12**):			
k_a	$8.6 \cdot 10^{9}$ 1/M·h	k_i	$4.3 \cdot 10^{9}$ 1/M·h
TTC (**7–9** and **S13** and **S14**):			
K	0.058 μM		
β_a	$\mu^{-1} \times 0.58$ μM	β_r	$\mu^{-1} \times 0.29$ μM
τ	5 h	σ_τ	0.5 h
RpaA activation TTC-only (**11** and **S16**):			
k_a^t	1 1/M·h	k_i^t	100 1/M·h
Minimal PPC (**S17–S20**):			
k_{dps}, $\tilde{k}_{dps}$	0.375 1/h	k_{pf}	1.0 1/h
f_6	100 1/h	b_0	90 1/h
k_i^{Af}	$1.72 \cdot 10^{10}$ 1/M·h	k_i^{Ab}	$\{1,3,9,27,81,243,729\}$ 1/h
$\tilde{k}_i^{Af}$	$1.72 \cdot 10^{9} \times \{10^{-2},10^{3},10^{3},10^{3},10^{2},10^{-3},10^{-4}\}$ 1/M·h		
$\tilde{k}_i^{Ab}$	$\{10^{6},10^{3},10^{-2},10^{-3},10^{-3},10^{-3},10^{3}\}$ 1/h		
Minimal TTC (**S21–S23**):			
K	0.29 μM	β_a	$\mu^{-1} \times 0.58$ μM
τ	8 h	σ_τ	0.8 h

The degradation rate μ is a free parameter that we vary to explore different growth conditions. The numbers between the curly brackets correspond to the different KaiC phosphorylation states i in ascending order; values of ∞ for K_i indicate that a particular binding reaction is not allowed. The production rate β_c is determined from an optimization for the mean protein concentration $\langle[C]\rangle = 0.58$ μM.

Table S2. Models with different output pathways from the PPC to the TTC

Model	Activator	Repressor	Threshold K	$n_{1/2}$
a	AC_2, AC_3, AC_4, AC_5	$A_yB_x\tilde{C}_2,\ldots,A_yB_x\tilde{C}_5$	0.058 μM	195
b	AC_3, AC_4	$A_yB_x\tilde{C}_2,\ldots,A_yB_x\tilde{C}_6$	0.058 μM	118
c	AC_3, AC_4	$A_yB_x\tilde{C}_3,\ldots,A_yB_x\tilde{C}_4$	0.058 μM	180
d	C_3, AC_3,C_4, AC_4	$A_yB_x\tilde{C}_3,\ldots,A_yB_x\tilde{C}_4$	0.029 μM	39
e	C_x, AC_x, $x \in \{2,3,4,5\}$	$A_yB_x\tilde{C}_3,\ldots,A_yB_x\tilde{C}_4$	0.029 μM	48

These models differ in the choice of phosphoforms that activate and repress RpaA, respectively. The maximal production rate β_c has been modified such that the average concentration of KaiC is 0.58 μM, as used in the in vitro experiments (3, 4). In each case, $n_{1/2}$ is given for a volume $V = 1$ μm³ and a decay rate $\mu = 0.03$ h^{-1}. Model a is the *PPC-TTC* model from the main text. To make the simulations tractable, we neglected repression of RpaA activation by KaiC phosphoforms that occur in negligible concentrations; consequently, the full list of phosphoforms that has the potential to repress RpaA is $\{B_2\tilde{C}_6,\ B_2\tilde{C}_5,AB_2\tilde{C}_5,A_2B_2\tilde{C}_5,\ B_2\tilde{C}_4,\ AB_2\tilde{C}_4,\ A_2B_2\tilde{C}_4,\ B_2\tilde{C}_3,\ AB_2\tilde{C}_3,\ A_2B_2\tilde{C}_3,\ B_2\tilde{C}_2,\ AB_2\tilde{C}_2,\ A_2B_2\tilde{C}_2\}$. Other parameters are given in Table S1